

Predictive Inference With Fast Feature Conformal Prediction

Zihao Tang

School of Statistics and Management
Shanghai University of Finance and Economics
tangzihao@stu.sufe.edu.cn

Boyuan Wang

School of Economics and Management
Tiangong University
2110610065@tiangong.edu.cn

Chuan Wen

Institute for Interdisciplinary Information Sciences
Tsinghua University
cwen20@mails.tsinghua.edu.cn

Jiaye Teng*

School of Statistics and Management
Shanghai University of Finance and Economics
tengjiaye@sufe.edu.cn

Abstract

Conformal prediction is widely adopted in uncertainty quantification, due to its post-hoc, distribution-free, and model-agnostic properties. In the realm of modern deep learning, researchers have proposed Feature Conformal Prediction (FCP), which deploys conformal prediction in a feature space, yielding reduced band lengths. However, the practical utility of FCP is limited due to the time-consuming non-linear operations required to transform confidence bands from feature space to output space. In this paper, we introduce Fast Feature Conformal Prediction (FFCP), which features a novel non-conformity score and is convenient for practical applications. FFCP serves as a fast version of FCP, in that it equivalently employs a Taylor expansion to approximate the aforementioned non-linear operations in FCP. Empirical validations showcase that FFCP performs comparably with FCP (both outperforming the vanilla version) while achieving a significant reduction in computational time by approximately 50x. The code is available at <https://github.com/ElvisWang1111/FastFeatureCP>

*Corresponding author.

1 Introduction

Machine learning has been successfully applied into various fields (Jordan and Mitchell, 2015; Silver et al., 2017). However, machine learning models often face overconfidence issues (Wei et al., 2022) and even hallucinations in large language models (LLMs) (Ji et al., 2023), which makes them unreliable and cannot be deployed in fields like finance and medicines (Gelijns et al., 2001; Thirumurthy et al., 2019; Morduch and Schneider, 2017). Therefore, it is essential to develop techniques for uncertainty quantification and calibrate the original model Abdar et al. (2021); Guo et al. (2017); Chen et al. (2021); Gawlikowski et al. (2021) Among the uncertainty quantification techniques, Conformal Prediction (Vanilla CP or split conformal prediction, Vovk et al. (2005); Shafer and Vovk (2008a); Burnaev and Vovk (2014)) stands out, because it is distribution-free, does not require retraining, and can be directly applied to various models. Conformal prediction uses a calibration step to calibrate a base model and then construct the confidence band. The goal of conformal prediction is to return a band $\mathcal{C}_{1-\alpha}$ such that

$$\mathbb{P}(Y' \in \mathcal{C}_{1-\alpha}(X')) \geq 1 - \alpha. \quad (1)$$

where (X', Y') is a test point and $1 - \alpha$ represents the confidence level.

In deep learning regimes, researchers try to utilize feature information in Vanilla CP, since the feature space usually contains meaningful semantic information in neural networks (Shen et al., 2014). This leads to Feature Conformal Prediction (FCP, Teng et al. (2022)). Fortunately, one may get different band lengths on different individuals by using the feature information, leading to a shorter confidence band. For comparison, on the regression task, Vanilla CP only returns the same band length for all individuals, which indicates a longer length. We refer to Teng et al. (2022) for more discussion.

However, the practical applications of FCP are limited because (a) it is time-consuming, and (b) it only returns *estimated* bands on the output space, making it less efficient. These two issues come from the step *Band Estimation*, which transfers the confidence band from feature space to output space. This step involves complex non-linear operations called LiPRA (Xu et al., 2020) and therefore (a) the non-linear operation requires high computational costs, and (b) the configurations in LiPRA might finally influence the estimated band, further harming the performance of FCP.

In this paper, we present Fast Feature Conformal Prediction (FFCP), which offers a fast version for handling the aforementioned nonlinear operations. Different from Vanilla CP and FCP, FFCP introduces a novel non-conformity score $s_{\text{ff}}(\cdot)$ that is simple to compute and does not require additional training,

$$s_{\text{ff}}(X, Y, g \circ h) = |Y - g \circ h(X)| / \|\nabla g(\hat{v})\|, \quad (2)$$

where (X, Y) denotes a sample, $g \circ h$ denotes a neural network where h denotes the feature layers and g denotes the prediction head, and the gradient $\nabla g(\hat{v})$ denotes the gradient of

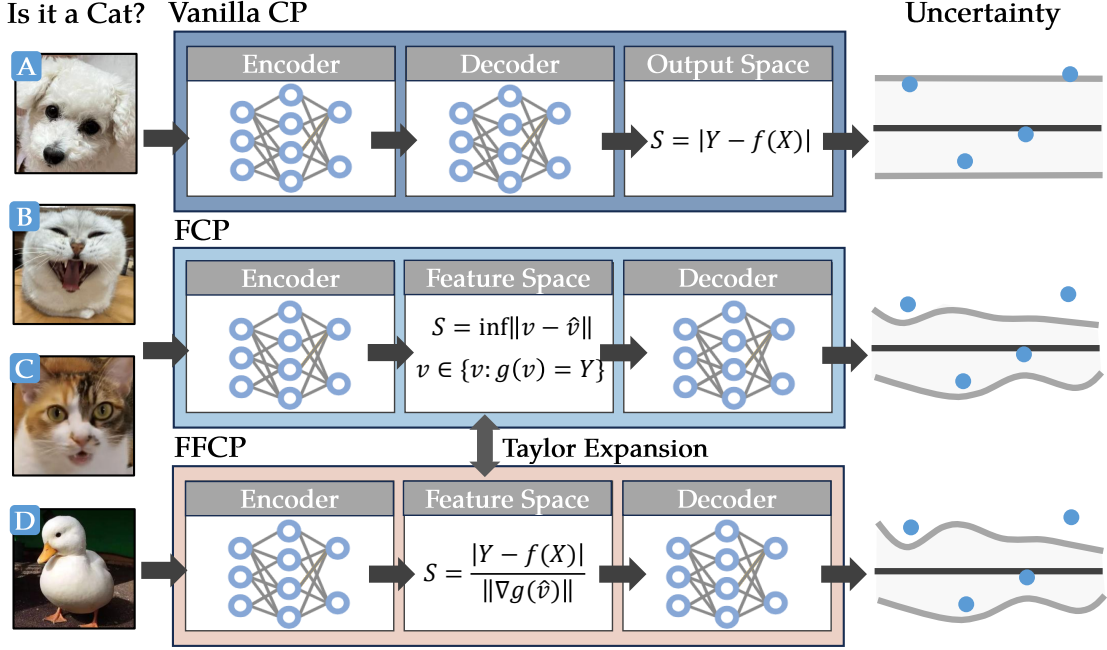


Figure 1: Comparison among Vanilla CP, FCP, and FFCP. FCP and FFCP are more efficient compared to Vanilla CP since they return different band lengths for different individuals. This is done by calculating a non-conformity score in the feature space. Besides, FFCP approximates FCP using a Taylor expansion, which leads to a different non-conformity score and accelerates the transformation from feature space to output space.

$g(\cdot)$ on the feature $\hat{v}_i \triangleq h(X)$, namely, $\nabla g(\hat{v}_i) = \frac{dg \circ h(X_i)}{dh(X_i)}$. We refer to Algorithm 2 for more details and illustrate the algorithm in Figure 1.

The above non-conformity score is closely related to FCP. Specifically, **FFCP using this non-conformity score can be regarded as a fast version of FCP, since it equivalently approximates the prediction head using a Taylor expansion**, which simplifies the aforementioned nonlinear operations. Fortunately, FFCP inherits the merits of FCP, for example, it also utilizes the semantic information in the feature. We refer to Section 5.4 for more discussion.

In the theoretical perspective, we first demonstrate that FFCP is effective in Theorem 4, in that it returned a confidence band with empirical coverage larger than the given confidence $1 - \alpha$. Additionally, we demonstrate in Theorem 5 that under square conditions, FFCP produces a shorter confidence band than Vanilla CP. The square conditions outline the properties of the feature space from two perspectives: expansion and quantile stability, implying that the feature space has a smaller distance between individual non-conformity scores and their quantiles. This reduces the cost of the quantile operation and therefore

leads to a shorter confidence band. We validate the square conditions using empirical observations.

Empirically, we conduct several experiments on real-world datasets and show that FFCP performs comparably with FCP, both outperforming Vanilla CP, **while achieving nearly 50 times the speed of FCP in terms of runtime** for regression tasks. We further validate the approximation ability of FFCP with FCP using the correlation between the non-conformity score of FFCP and FCP. We also apply FFCP to the image segmentation problems to verify its general applications. Besides, we show that the concept in FFCP is pretty general, and can be combined with other variants of CP, *e.g.*, CQR (Romano et al., 2019a) and LCP (Guan, 2023) in regression tasks, and RAPS (Angelopoulos et al., 2020) in classification tasks.

Overall, our main contributions are summarized as follows:

- We propose FFCP, which serves as a fast version of FCP. FFCP approximately achieves a 50x reduction in running time compared to FCP (Table 1) by using a Taylor expansion to approximate the prediction head in FCP. Besides, FFCP inherits the merits of FCP and efficiently exploits semantic information in the feature space like FCP.
- Theoretical insights demonstrate that FFCP returns shorter band length compared to Vanilla CP (Theorem 5) while ensuring coverage exceeds the given confidence level under some mild conditions (Theorem 4).
- Extensive experiments with both synthetic and real data demonstrate the effectiveness of the proposed FFCP algorithm (Table 2). Additionally, we demonstrate the universal applicability of our gradient-level techniques by extending them to other tasks such as classification (FFRAPS, Algorithm 5) and segmentation, and to various conformal prediction variants, including CQR (FFCQR, Algorithm 3) and LCP (FFLCP, Algorithm 4).

2 Related Work

Conformal prediction is a post-hoc calibration method dealing with uncertainty quantification (Vovk et al., 2005; Shafer and Vovk, 2008b; Barber et al., 2020), which is deployed in numerous fields (Ye et al., 2024; Kumar et al., 2023; Quach et al., 2023). The variants of conformal prediction typically revolve around the concept of non-conformity scores, with four main branches of development.

Relaxing Exchangeability. The first branch relaxes the exchangeability requirement (Tibshirani et al., 2019a; Hu and Lei, 2020; Podkopaev and Ramdas, 2021; Barber et al., 2022),

leveraging weighted or reweighted quantiles to relax exchangeability. By doing so, it gains more flexibility and broader applicability in handling data that may not satisfy the standard exchangeability assumptions.

Diverse Structures. The second branch applies conformal prediction to various data structures, for example, classification tasks (Romano et al., 2020; Angelopoulos et al., 2020), time series data (Xu and Xie, 2021; Gibbs and Candès, 2021), censored data in survival analysis (Teng et al., 2021; Candès et al., 2023), high-dimensional data (Candès et al., 2021; Lei et al., 2013), Bellman-based data (Yang et al., 2024), counterfactuals and individual treatment effects (Lei and Candès, 2021), and so on.

Another way involves model structures, such as k -NN regression (Papadopoulos et al., 2011a), quantiles incorporated (Romano et al., 2019b; Sesia and Candès, 2020), density estimators (Izbicki et al., 2020a), and conditional histograms (Sesia and Romano, 2021). These methods further enrich the application scenarios of conformal prediction by adapting it to diverse model frameworks.

Enhancing Methods. The third branch focuses on enhancing the original conformal prediction with band length. Izbicki et al. (2020b) introduce CD-split and HPD-split methods, and Yang and Kuchibhotla (2021) develop selection methods to minimize band length. Of particular note is feature conformal prediction (Teng et al., 2022), which leverages neural network training information via feature spaces to improve band length.

Localized Conformal Prediction. The fourth branch focuses on enhancing the non-conformity score normalization by incorporating difficulty-related terms like $\frac{\|Y - \hat{Y}\|}{\sigma(X')}$ where Y denotes the true label, \hat{Y} denotes the predicted label, and $\sigma(X')$ denotes the standard deviation related to X' . Here are three key approaches:

1. **Weight Adjustment via Calibration Distances.** This approach mainly calculates the distance from the testing point to the calibration points and then uses these distances to define the weights of non-conformity scores in the calibration process (Han et al., 2022; Guan, 2023). Our gradient-level techniques can be used to combine with this branch (see FFLCP proposed later).
2. **Normalization Using Proximity to Training Set.** This approach utilizes the observation that a testing point exhibits smaller uncertainty when it is close to the training set, and uses such metrics to approximate $\sigma(X')$ (Papadopoulos et al., 2008, 2011b; Papadopoulos and Haralambous, 2011). In the deep learning regimes, we believe that such procedures can be further improved by calculating the distance in the feature space rather than the input space, since feature layers usually contain more semantic information.

3. **Modeling** $\sigma(X')$. A model is trained to estimate $\sigma(X')$, offering computational efficiency and reducing the need for additional training data (Seedat et al., 2023, 2024).

Uncertainty Quantification. Uncertainty quantification is one of the most fundamental questions in machine learning. In addition to conformal prediction (CP) methods, many other approaches exist for quantifying uncertainty. Common techniques include calibration-based techniques (Guo et al., 2017; Kuleshov et al., 2018; Nixon et al., 2019; Abdar et al., 2021; Chang et al., 2024) and Bayesian-based techniques (Blundell et al., 2015; Hernández-Lobato and Adams, 2015; Li and Gal, 2017; Izmailov et al., 2021; Jospin et al., 2022).

3 Preliminaries

We begin by introducing a dataset $\mathcal{D} = \{(X_i, Y_i)\}_{i \in [n]}$ indexed by \mathcal{I} . We split the dataset into two folds: a training fold \mathcal{D}_{tra} indexed by \mathcal{I}_{tra} , and a calibration fold \mathcal{D}_{cal} indexed by \mathcal{I}_{cal} . Denote the testing point by (X', Y') . For the model part, define f as a neural network. We partition $f = g \circ h$, where h denotes the feature function (the initial layers of the neural network) and g denotes the prediction head. For a sample (X, Y) , we define $\hat{v} = h(X)$ as the trained feature. We follow the ideas in Teng et al. (2022) and define the surrogate feature as any feature v such that $g(v) = Y$.

Assumption 1 (exchangeability). *Assume that the calibration data $(X_i, Y_i) \in \mathcal{D}_{\text{cal}}$ and the testing point (X', Y') are exchangeable. Formally, define $Z_i, i = 1, \dots, |\mathcal{I}_{\text{cal}}| + 1$, as the above data pair. Then Z_i are exchangeable if arbitrary permutation follows the same distribution, i.e.,*

$$(Z_1, \dots, Z_{|\mathcal{I}_{\text{cal}}|+1}) \stackrel{d}{=} (Z_{\pi(1)}, \dots, Z_{\pi(|\mathcal{I}_{\text{cal}}|+1)}), \quad (3)$$

with arbitrary permutation π over $\{1, \dots, |\mathcal{I}_{\text{cal}}| + 1\}$.

Typically, Vanilla CP is composed of three key steps.

I. Training Step. We first train a base model using the training fold \mathcal{D}_{tra} .

II. Calibration Step. We calculate a non-conformity score $R_i = |Y_i - f(X_i)|$ using the calibration fold \mathcal{D}_{cal} . The form of the score function might vary case by case, quantifying the divergence between ground truth and predicted values.

III. Testing Step. We construct the confidence band for the testing point (X', Y') using the quantile of the non-conformity score $Q_{1-\alpha}$.

We present Vanilla CP in Algorithm 1¹, and provide its theoretical guarantee in Theorem 2.

Theorem 2. *Under Assumption 1, the confidence band $\mathcal{C}_{1-\alpha}(X')$ returned by Algorithm 1*

¹ δ represents the Dirac function.

Algorithm 1 Vanilla Conformal Prediction

Input: Confidence level α , dataset $\mathcal{D} = \{(X_i, Y_i)\}_{i \in \mathcal{I}}$, testing point X'

- 1: Randomly split the dataset \mathcal{D} into a training fold $\mathcal{D}_{\text{tra}} \triangleq \{(X_i, Y_i)\}_{i \in \mathcal{I}_{\text{tra}}}$ and a calibration fold $\mathcal{D}_{\text{cal}} \triangleq \{(X_i, Y_i)\}_{i \in \mathcal{I}_{\text{cal}}}$;
- 2: Train a base model $f(\cdot)$ with training fold \mathcal{D}_{tra} ;
- 3: For each $i \in \mathcal{I}_{\text{cal}}$, calculate the non-conformity score $R_i = |Y_i - f(X_i)|$;
- 4: Calculate the $(1 - \alpha)$ -th quantile $Q_{1-\alpha}$ of the distribution $\frac{1}{|\mathcal{I}_{\text{cal}}|+1} \sum_{i \in \mathcal{I}_{\text{cal}}} \delta_{R_i + \delta_\infty}$.

Output: $\mathcal{C}_{1-\alpha}^{\text{Vanillacp}}(X') = [f(X') - Q_{1-\alpha}, f(X') + Q_{1-\alpha}]$.

satisfies

$$\mathbb{P}(Y' \in \mathcal{C}_{1-\alpha}(X')) \geq 1 - \alpha. \quad (4)$$

4 Methodology

In this section, we first illustrate the motivation behind FFCP in Section 4.1. Specifically, we address the complexity of non-linear operators in FCP and provide how we derive FFCP from FCP. We then formally present the specific form of FFCP, including the non-conformity score, the returned bands, and the corresponding pseudocode. We finally provide theoretical analyses on the coverage and band length in Section 4.2.

4.1 Relationship between FFCP and FCP

In this section, we discuss the motivation behind FFCP. FFCP is inspired by FCP (Teng et al., 2022), which conducts conformal prediction in the feature space. However, since the band is constructed in the feature space, FCP requires a *Band Estimation* process to go from feature space to output space. Specifically, FCP applies *LiPRA* (Xu et al., 2020) which derives the band in the output space $\{g(v) : \|v - \hat{v}\| \leq Q_{1-\alpha}\}$. Unfortunately, the exact band is difficult to represent explicitly since the prediction head g is usually highly non-linear, thereby resulting in significant computational complexity in terms of time. Therefore, we propose approximating g using a first-order Taylor expansion to simplify the aforementioned non-linear operator.

The core steps of FCP include: (a) calculating the non-conformity score (from output space to feature space), followed by (b) deriving the confidence band (from feature space to output space). We next introduce the concrete formulation of how FFCP approximates FCP.

From output space to feature space. FCP uses the non-conformity score $s_f(\cdot)$ in the feature space

$$s_f(X, Y, g \circ h) = \inf_{v \in \{v: g(v)=Y\}} \|v - \hat{v}\|. \quad (5)$$

By using the Taylor expansion, one approximates g with $g(v) \approx g(\hat{v}) + \nabla g(\hat{v})(v - \hat{v})$. Plugging into the approximation of g leads to a new non-conformity score $s_{\text{ff}}(\cdot)$

$$s_{\text{ff}}(X, Y, g \circ h) = |Y - f(X)| / \|\nabla g(\hat{v})\|, \quad (6)$$

where $\nabla g(\hat{v})$ denotes the gradient of $g(\hat{v})$ on the feature \hat{v} , namely $\nabla g(\hat{v}) = \frac{dg \circ h(X)}{dh(X)}$.

From feature space to output space. After constructing the confidence band in the feature space, FCP maps this band to the output space. Specifically, they derive the following band in the output space which is called *Band Estimation*:

$$\{g(v) : \|v - \hat{v}\| \leq Q_{1-\alpha}\}. \quad (7)$$

They propose to use LiPRA in this process, which is time-consuming. By plugging into the Taylor approximation of g , one can construct the band $\mathcal{C}_{1-\alpha}^{\text{ffcp}}$ as

$$\mathcal{C}_{1-\alpha}^{\text{ffcp}}(X) = [g(\hat{v}) - \|\nabla g(\hat{v})\|Q_{1-\alpha}, g(\hat{v}) + \|\nabla g(\hat{v})\|Q_{1-\alpha}]. \quad (8)$$

Remark 3 (High-dimensional Response). When the response $Y = [Y^1, Y^2, \dots, Y^m]$ is high-dimensional, one can deploy conformal prediction in a coordinate-wise level. In this scenario, the confidence band for a specific dimension $j \in [m]$ of Y becomes

$$s_{\text{ff}}^j(X, Y, g \circ h) = |Y^j - f(X)^j| / \|\nabla g(\hat{v})^j\|, \quad (9)$$

where $\nabla g(\hat{v})^j = \left(\frac{\partial f(X)}{\partial h(X)}\right)_j$ represents the j -th row of the Jacobian matrix of f with respect to h at X . And the returned band for the j -th coordinate is derived as follows:

$$\mathcal{C}_{1-\alpha}^{\text{ffcp}}(X)_j = [g(\hat{v})^j - \|\nabla g(\hat{v})^j\|Q_{1-\alpha}, g(\hat{v})^j + \|\nabla g(\hat{v})^j\|Q_{1-\alpha}]. \quad (10)$$

Based on the above discussion, we present the full algorithm in Algorithm 2. Notably, the Taylor expansion in FFCP is usually different for each sample X, Y , which further leads to confidence bands that are individually different. Besides, FFCP inherits the advantages of FCP. For example, this framework is pretty general and can be combined with other variants of Vanilla CP, *e.g.*, CQR (Romano et al., 2019a).

4.2 Theoretical Guarantee for FFCP

This section outlines the theoretical guarantee for FFCP concerning coverage (effectiveness) and band length (efficiency). Below, we offer the main theorems and defer the full proofs to Appendix A.1 and A.2.

We first demonstrate that the confidence band produced by Algorithm 2 is valid under Assumption 1.

Algorithm 2 Fast Feature Conformal Prediction

Input: Confidence level α , dataset $\mathcal{D} = \{(X_i, Y_i)\}_{i \in \mathcal{I}}$, testing point X'

- 1: Randomly split the dataset \mathcal{D} into a training fold $\mathcal{D}_{\text{tra}} \triangleq \{(X_i, Y_i)\}_{i \in \mathcal{I}_{\text{tra}}}$ and a calibration fold $\mathcal{D}_{\text{cal}} \triangleq \{(X_i, Y_i)\}_{i \in \mathcal{I}_{\text{cal}}}$;
- 2: Train a base neural network with training fold $f(\cdot) = g \circ h(\cdot)$ with training fold \mathcal{D}_{tra} ;
- 3: For each $i \in \mathcal{I}_{\text{cal}}$, calculate the non-conformity score $\tilde{R}_i = |Y_i - f(X_i)| / \|\nabla g(\hat{v}_i)\|$, where $\nabla g(\hat{v}_i)$ denotes the gradient of $g(\cdot)$ on the feature $\hat{v}_i \triangleq h(X_i)$, namely $\nabla g(\hat{v}_i) = \frac{dg \circ h(X_i)}{dh(X_i)}$;
- 4: Calculate the $(1 - \alpha)$ -th quantile $Q_{1-\alpha}$ of the distribution $\frac{1}{|\mathcal{I}_{\text{cal}}|+1} \sum_{i \in \mathcal{I}_{\text{cal}}} \delta_{\tilde{R}_i} + \delta_\infty$;

Output: $\mathcal{C}_{1-\alpha}^{\text{ffcp}}(X') = [f(X') - \|\nabla g(\hat{v}')\|Q_{1-\alpha}, f(X') + \|\nabla g(\hat{v}')\|Q_{1-\alpha}]$, where $\hat{v}' = h(X')$.

Theorem 4 (Coverage). *Under Assumption 1, for any $\alpha > 0$, the confidence band returned by Algorithm 2 satisfies:*

$$\mathbb{P}(Y' \in \mathcal{C}_{1-\alpha}^{\text{ffcp}}(X')) \geq 1 - \alpha, \quad (11)$$

where the probability is taken over the calibration fold and the testing point (X', Y') .

Next, we show that FFCP is provably more efficient than the Vanilla CP. To simplify the discussion, we present an informal version of Theorem 5 here and postpone the formal version to Appendix A.2.

Theorem 5 (Band Length). *Under mild assumptions, if the following square conditions hold:*

1. **Expansion.** *The feature space expands the differences between individual length and their quantiles.*
2. **Quantile Stability.** *Given a calibration set \mathcal{D}_{cal} , the quantile of the band length is stable in both feature space and output space.*

Then FFCP provably outperforms vanilla CP in terms of average band length.

Theorem 5 implies that FFCP provably outperforms Vanilla CP in terms of average band length. The *square conditions* imply that the feature space has a smaller distance between individual non-conformity scores and their quantiles. This reduction in the computational overhead of the quantile operation subsequently yields a shorter band length. We provide empirical verifications on this assumption, see Figure 4 for more details.

The intuition behind Theorem 5 is as follows: Initially, FFCP and Vanilla CP perform quantile operations in different spaces, with the *Expansion* condition ensuring that the quantile step in FFCP costs less. The ultimate *Quantile Stability* condition confirms that the band can be generalized from the calibration folds to the test folds.

5 Experiments

This section presents the experiments to validate the utility of FFCP. Firstly, we detail the experimental setup in Section 5.1. Secondly, we present that FFCP achieves both effectiveness and efficiency with faster execution in Section 5.2. Thirdly, in Section 5.3.1, we verify that FFCP can be easily deployed and performs robustly across various tasks, including classification and segmentation. Furthermore, in Section 5.3.2, we show that the gradient-level techniques used in FFCP can be extended to classic CP models such as CQR (Romano et al., 2019a) and LCP (Guan, 2023). A more detailed account of this extension can be found in Section 5.3. Finally, we conduct several more experiments in Section 5.4 to establish the close relationship between FFCP and FCP, to demonstrate the benefits of FFCP from the good representation of gradient, and to provide empirical validations for the theoretical insights.

5.1 Experiments Setups

Datasets. We consider both synthetic datasets and realistic datasets, including **(a) synthetic dataset:** $Y = WX + \epsilon$, where $X \in [0, 1]^{100}$, $Y \in \mathbb{R}$, $\epsilon \sim \mathcal{N}(0, 1)$, W is a fixed randomly matrix. **(b) real-world unidimensional target datasets:** ten datasets from UCI machine learning (Asuncion, 2007) and other sources: community and crimes (*COM*), Facebook comment volume variants one and two (*FBI* and *FB2*), medical expenditure panel survey (*MEPS19–21*) (Cohen et al., 2009), Tennessee’s student teacher achievement ratio (*STAR*) (Achilles et al., 2008), physicochemical properties of protein tertiary structure (*BIO*), blog feedback (*BLOG*) (Buza, 2014), and bike sharing (*BIKE*). and **(c) real-world semantic segmentation dataset:** Cityscapes (Cordts et al., 2016). **(d) real-world semantic classification dataset:** Imagenet-Val.

Algorithms. We compare three methods: Vanilla CP, FCP, and FFCP, with Vanilla CP serving as the baseline. For the one-dimensional scenario, we perform direct calculations. For higher-dimensional cases, we use a coordinate-wise level non-conformity score.

Evaluation. The algorithmic empirical performance is evaluated with the following metrics:

- **Runtime** For runtime evaluation of the algorithm, the timing starts at the score calculation and ends with the final prediction bands returned. All the tests are performed on a desktop with an Intel Core i9-12900H CPU, NVIDIA GeForce RTX 4090 GPU, and 32 GB memory.
- **Coverage (Effectiveness)** Coverage refers to the observed frequency with which a test point falls within the predicted confidence interval. Ideally, a predictive inference method should yield a coverage rate that is slightly higher than $1 - \alpha$ for a given confidence level α .

Table 1: Time comparison among Vanilla CP, FCP, and FFCP. FFCP ensures faster running speed compared to FCP. The last column represents the speed improvement factor of FFCP compared to FCP. The time unit is in seconds.

DATASET	VANILLA CP	FCP	FFCP	FASTER
SYNTHETIC	0.0088±0.0003	3.8939±0.3725	0.0902±0.0056	43X
COM	0.0047±0.0010	4.9804±0.8588	0.0844±0.0187	59X
FB1	0.0245±0.0059	5.9822±0.9871	0.1940±0.0564	31X
FB2	0.0414±0.0070	9.3534±0.0927	0.2510±0.0058	37X
MEPS19	0.0106±0.0010	3.3237±0.0431	0.0755±0.0037	44X
MEPS20	0.0152±0.0016	5.4003±0.3945	0.0948±0.0077	57X
MEPS21	0.0137±0.0008	4.1657±0.0670	0.0854±0.0146	49X
STAR	0.0030±0.0006	3.5842±0.3722	0.0332±0.0066	108X
BIO	0.0291±0.0053	7.5417±1.1028	0.2042±0.0344	37X
BLOG	0.0340±0.0024	8.0913±1.2072	0.2239±0.0261	36X
BIKE	0.0072±0.0007	3.5806±0.0285	0.0534±0.0021	67X

- **Band length (Efficiency)** When the coverage exceeds $1 - \alpha$, our goal is to minimize the length of the confidence band. For FFCP, since we use a 5-layer neural network, each layer can be viewed as a feature layer. Therefore, in the experiments, we obtain the band length returned by each of the 5 layers of the neural network. In the subsequent results, if only a single band length is presented, it corresponds to the shortest band length returned by the different neural network layers. Otherwise, the results for all layers from layer 0 to layer 4 (with the last layer typically representing the Vanilla CP result) will be shown.

Let $Y = (Y^1, \dots, Y^d) \in \mathbb{R}^d$ denote the d -dimensional response variable, and let $\mathcal{C}(X) \subseteq \mathbb{R}^d$ be the confidence band associated with predictor X . The length of this confidence band in each dimension is represented by the vector $|\mathcal{C}(X)| = (|\mathcal{C}(X)|^1, \dots, |\mathcal{C}(X)|^d) \in \mathbb{R}^d$. Denote the indices of the test set by \mathcal{I}_{tes} and the set of dimensions by $[d] = \{1, \dots, d\}$.

We then define the coverage and band length as:

$$\text{Coverage} = \frac{1}{|\mathcal{I}_{\text{tes}}|} \sum_{i \in \mathcal{I}_{\text{tes}}} \mathbb{I}(Y_i \in \mathcal{C}(X_i)), \quad \text{Band Length} = \frac{1}{|\mathcal{I}_{\text{tes}}|} \sum_{i \in \mathcal{I}_{\text{tes}}} \left(\frac{1}{d} \sum_{j=1}^d |\mathcal{C}(X_i)|^j \right), \quad (12)$$

where $\mathbb{I}(\cdot)$ is the indicator function that equals 1 if its argument is true and 0 otherwise.

5.2 Results on Coverage, Band Length and Runtime

Runtime Comparison. The runtime comparison is presented in Table 1. The results show that FFCP outperforms FCP with an approximate 50x speedup in runtime. Notably, since

Table 2: Comparison of coverage and band length among Vanilla CP, FCP, and FFCP. FFCP achieves significantly faster running speeds while performing comparably to FCP in most datasets and outperforming Vanilla CP. For FFCP, we select the shortest band length among all layers.

METHOD	VANILLA CP		FCP		FFCP	
	COVERAGE	LENGTH	COVERAGE	LENGTH	COVERAGE	LENGTH
SYNTHETIC	90.080±0.951	0.176±0.015	89.930±0.956	0.081 ±0.041	90.080±0.951	0.176±0.015
COM	89.875±0.985	1.974±0.071	89.724±1.087	1.939±1.408	90.226±2.179	1.838 ±0.180
FB1	90.254±0.170	2.004±0.191	90.198±0.207	2.010±0.182	90.168±0.220	1.472 ±0.232
FB2	89.933±0.206	2.016±0.218	89.966±0.130	1.371 ±0.370	89.868±0.062	1.425±0.109
MEPS19	90.567±0.311	3.982±0.614	90.605±0.340	3.493±2.734	90.352±0.469	3.134 ±0.309
MEPS20	89.923±0.715	4.184±0.316	89.929±0.770	2.730 ±0.962	89.615±0.661	3.268±0.283
MEPS21	90.019±0.341	3.732±0.555	90.038±0.303	3.393±1.313	89.745±0.344	3.146 ±0.506
STAR	90.393±1.494	0.208±0.004	90.300±1.362	0.174 ±0.038	90.393±1.494	0.208±0.004
BIO	89.875±0.488	1.661±0.019	89.930±0.501	1.412 ±0.265	89.875±0.488	1.661±0.019
BLOG	90.176±0.241	3.524±0.850	90.151±0.405	2.795±1.385	90.059±0.101	2.741 ±0.517
BIKE	89.871±0.568	0.703±0.016	89.394±0.633	2.147±0.249	89.624±0.688	0.635 ±0.030

Vanilla CP is the most basic method and does not utilize additional tools, it exhibits the fastest runtime.

Coverage. Table 2 summarizes the coverage for the one-dimensional response. Experimental results indicate that the coverage of FFCP all exceeds the confidence level $1 - \alpha$, affirming its effectiveness as stated in Theorem 4.

Band Length. The band length is detailed in Table 2 for a one-dimensional response. It is noteworthy that FFCP surpasses Vanilla CP by achieving a shorter band length, thereby validating the efficiency of the algorithm.

5.3 Extensions of FFCP

This section provides the extensions of FFCP, which is divided into two parts. Section 5.3.1 mainly discusses the applications of FFCP beyond regression tasks, specifically in image classification (Angelopoulos et al., 2020) and segmentation tasks. Section 5.3.2 focuses on how the gradient-level techniques in FFCP can be extended to other CP variants, *e.g.*, CQR (Romano et al., 2019a) and LCP (Guan, 2023).

5.3.1 Other Tasks

Classification. We extend the FFCP techniques to classification tasks using the baseline RAPS (Angelopoulos et al., 2020) model, creating a new variant called FFRAPS (Fast Feature RAPS, Algorithm 5 in Appendix B.7). According to the experimental findings

Table 3: Comparison of FFRAPS with the state-of-the-art method RAPS on Imagenet-Val. The FFRAPS method outperforms RAPS in most datasets.

METHOD MODEL	ACCURACY		COVERAGE		LENGTH	
	TOP-1	TOP-5	RAPS	FFRAPS	RAPS	FFRAPS
RESNEXT101	0.793±0.001	0.945±0.001	0.908±0.002	0.907±0.002	2.012±0.035	2.006 ±0.039
RESNET152	0.784±0.001	0.941±0.001	0.909±0.003	0.907±0.003	2.144±0.034	2.128 ±0.058
RESNET101	0.774±0.001	0.935±0.001	0.906±0.004	0.906±0.003	2.348±0.151	2.256 ±0.037
RESNET50	0.761±0.001	0.929±0.001	0.907±0.004	0.907±0.003	2.560 ±0.104	2.594±0.069
RESNET18	0.698±0.001	0.891±0.001	0.906±0.003	0.903±0.003	4.560±0.147	4.434 ±0.168
DENSENET161	0.772±0.001	0.936±0.001	0.907±0.003	0.907±0.002	2.374±0.083	2.328 ±0.056
VGG16	0.716±0.001	0.904±0.001	0.904±0.002	0.902±0.002	3.566±0.098	3.521 ±0.065
INCEPTION	0.696±0.001	0.887±0.001	0.903±0.003	0.903±0.002	5.410±0.350	5.407 ±0.133
SHUFFLENET	0.694±0.001	0.883±0.001	0.902±0.001	0.901±0.002	5.001±0.121	4.971 ±0.073

presented in Table 3, FFRAPS returns shorter band lengths while preserving the coverage compared to RAPS under most model structures.

Segmentation. The gradient-level techniques of FFCP also prove effective in segmentation tasks. The segmentation results in Figure 2 reveal that FFCP returns appropriate bands across different regions. Specifically, larger bands are observed in less informative areas, such as at object boundaries, whereas narrower bands are found in more informative regions. This validates the efficiency of FFCP in segmentation tasks.

5.3.2 Extending FFCP into Other Models

Conformalized Quantile Regression (CQR, Romano et al. (2019a)) The gradient-level techniques of FFCP are adaptable to other conformal prediction frameworks like CQR. We develop FFCQR (Fast Feature CQR, Algorithm 3 in Appendix B.5), which not only significantly reduces runtime compared to FCQR but also exhibits better performance than CQR. Additionally, we observe that for the neural network significant level setting $[\alpha, 1 - \alpha]$ in the CQR method, as the α value increases, approaching $1 - \alpha$, the performance of FFCQR gradually improves. For detailed experimental results in Table 8,9, 11, 10, 12 in the Appendix B.5.

Locally Adaptive Conformal Prediction (LCP, Guan (2023)) Integrating gradient-level techniques from FFCP into the LCP method leads to FFLCP (Fast Feature LCP, Algorithm 4 in Appendix B.6). Experimental results in Table 4 indicate that FFLCP outperforms LCP in terms of group coverage, highlighting an improvement in the adaptability of LCP to locally adaptive methods.

Table 4: Comparison of LCP and FFLCP in group coverage. We divide the datasets into three groups based on the size of Y , and calculate the coverage for each group, returning the maximum coverage. FFLCP shows the results for the 5-layer neural network.

METHOD	LCP		FFLCP				
	DATASET	COVERAGE	LAYER0	LAYER1	LAYER2	LAYER3	LAYER4
SYNTHETIC		87.02±1.00	86.93±0.78	86.57±0.88	85.43±1.24	87.11 ±1.76	87.02±1.00
COM		80.33±3.24	81.84 ±2.52	79.56±3.34	77.42±4.12	79.41±2.88	80.33±3.24
FB1		52.51±1.76	78.61 ±0.91	76.39±1.21	67.16±1.61	57.82±1.88	52.51±1.76
FB2		54.33±1.75	75.86 ±0.83	75.44±0.91	70.45±0.99	60.18±1.73	54.33±1.75
MEPS19		67.35±1.21	68.19 ±2.31	66.44±2.01	64.94±1.53	67.14±1.24	67.35±1.21
MEPS20		65.49±1.64	69.30 ±1.09	68.80±1.55	65.14±1.44	65.47±1.99	65.49±1.64
MEPS21		66.38±0.95	67.82±1.10	67.96 ±1.21	66.21±1.33	65.54±1.02	66.38±0.95
STAR		77.20±3.97	79.69 ±2.88	79.28±1.72	77.47±5.21	77.33±4.12	77.20±3.97
BIO		81.10±0.61	86.33±0.51	86.06±0.50	86.78 ±0.57	83.26±0.71	81.10±0.61
BLOG		48.99±1.01	61.01 ±0.82	55.10±1.12	46.01±0.65	46.88±0.81	48.99±1.01
BIKE		77.61±1.52	81.02±1.73	82.42±2.08	82.97±1.29	84.41 ±1.71	77.61±1.52

5.4 Discussion

Robustness for FFCP. The empirical performance of FFCP demonstrates its robustness, as seen in the ablation studies on splitting points. We demonstrate that coverage remains robust across different splitting points in neural networks, as detailed in Table 7 in Appendix B.3. Furthermore, the results from different layers of the FFCP network are consistent, as presented in Table 5

FFCP is similar to FCP. We compare the relationship between the scores of FCP and FFCP through experiments. Figure 3 indicates a positive correlation between the non-conformity scores of the two algorithms, suggesting that FFCP shares similarities with FCP in score function.

FFCP on untrained network. We propose that FFCP returns shorter band lengths through its deployment of deep representations from the gradients. To test this view, we contrast FFCP’s performance using an untrained neural network against a baseline model. Using an incompletely trained neural network, FFCP’s performance deteriorates and becomes comparable to that of Vanilla CP. This is due to the partially incorrect semantic information in the gradient, which *misleads* FFCP. We defer the results to Table 6 and related discussion to Appendix B.4.

Table 5: Coverage and Band Length based on Gradient from Different Layers of Neural Networks. FFCP LAYER(·) represents using the gradient between the LAYER(·) and the output. The results in LAYER4 are equivalent to Vanilla CP.

LAYER DATASET	LAYER1		LAYER2		LAYER3		LAYER4	
	COVERAGE	LENGTH	COVERAGE	LENGTH	COVERAGE	LENGTH	COVERAGE	LENGTH
SYNTHETIC	89.810±0.784	0.184±0.018	90.050±0.534	0.184±0.017	89.960±0.910	0.182 ±0.023	90.220±0.983	0.189±0.033
COM	90.476±1.889	1.878±0.224	90.226±2.179	1.838 ±0.180	89.674±1.465	1.853±0.136	89.825±0.646	2.037±0.188
FB1	90.112±0.199	3.540±0.327	90.212±0.357	2.860±0.327	90.083±0.216	1.597±0.052	90.168±0.220	1.472 ±0.232
FB2	89.953 ±0.250	3.530±0.384	89.897±0.235	3.048±0.510	89.956±0.159	2.077±0.517	89.868±0.062	1.425 ±0.109
MEPS19	90.155±0.643	3.251±0.396	90.352±0.469	3.134 ±0.309	90.440±0.183	3.184±0.482	90.586±0.246	3.795±0.640
MEPS20	89.934±0.520	4.302±1.377	89.889±0.621	3.573±0.488	89.615±0.661	3.268 ±0.283	89.82±0.689	3.817±0.308
MEPS21	89.496±0.262	3.443±0.487	89.623±0.275	3.218±0.239	89.745±0.344	3.146 ±0.506	90.026±0.301	3.452±0.711
STAR	90.901±1.732	0.221±0.002	90.993±1.807	0.217±0.003	91.039±1.442	0.210±0.004	90.300±1.248	0.209 ±0.004
BIO	89.937±0.391	2.292±0.077	90.022±0.375	2.042±0.067	89.991±0.594	2.080±0.063	90.127±0.476	1.822 ±0.025
BLOG	89.968±0.420	4.772±0.614	89.918±0.319	3.404±0.598	90.059±0.101	2.741 ±0.517	90.017±0.197	3.058±0.873
BIKE	89.917±0.791	1.701±0.254	89.568±0.476	1.138±0.114	89.495±0.579	0.794±0.068	89.624±0.688	0.635 ±0.030

6 Conclusion

In this paper, we propose FFCP, a gradient-based non-conformity score that serves as a faster alternative to FCP, achieving processing times 50 times faster than FCP. Theoretically, we have established the effectiveness and efficiency of FFCP under mild assumptions. In our experiments, we apply FFCP to a variety of tasks, including basic regression tasks, classification tasks with FFRAPS based on RAPS, and segmentation. Additionally, we introduce FFCQR based on CQR, as well as FFLCP based on LCP. These experimental results demonstrate the broad adaptability of our techniques.

For future work, the following points could be considered: (1) We use information from the first derivative and have not delved into higher-order derivatives, which may contain more feature information; (2) The computation of gradients becomes very costly as dimensionality increases, thus special methods are needed to handle large-scale tasks; and (3) The gradient at a single point may be unstable, especially when the gradient is zero, so methods such as random smoothing could be considered.

Table 6: Untrained model comparison between Vanilla CP and FFCP. When the model has not been sufficiently trained, FFCP performs similarly to Vanilla CP. This means that the model’s performance determines the quality of the feature information in the gradient. When the model performs poorly, the gradient information obtained by FFCP is inaccurate. On the other hand, this also suggests that FFCP effectively utilizes the feature information in the gradient when the model is well-trained.

METHOD	VANILLA CP		FFCP	
	COVERAGE	LENGTH	COVERAGE	LENGTH
SYNTHETIC	90.23±0.45	2.34 ±0.01	90.22±0.96	2.41±0.01
COM	90.33±1.81	4.86±0.13	90.43±1.99	4.73 ±0.08
FB1	90.18±0.19	3.57±0.09	90.10±0.13	3.57 ±0.08
FB2	90.16±0.11	3.66±0.11	90.12±0.14	3.66 ±0.06
MEPS19	90.80±0.43	4.33 ±0.07	90.85±0.58	4.38±0.07
MEPS20	90.15±0.55	4.41 ±0.23	90.27±0.63	4.46±0.25
MEPS21	89.80±0.45	4.41 ±0.17	89.89±0.56	4.41 ±0.15
STAR	89.79±0.51	1.88 ±0.01	89.98±0.56	1.94±0.01
BIO	90.16±0.20	4.09±0.02	90.07±0.14	4.04 ±0.02
BLOG	90.11±0.30	2.53 ±0.12	90.12±0.28	2.55±0.14
BIKE	89.55±0.82	4.56 ±0.09	89.57±0.86	4.60±0.10

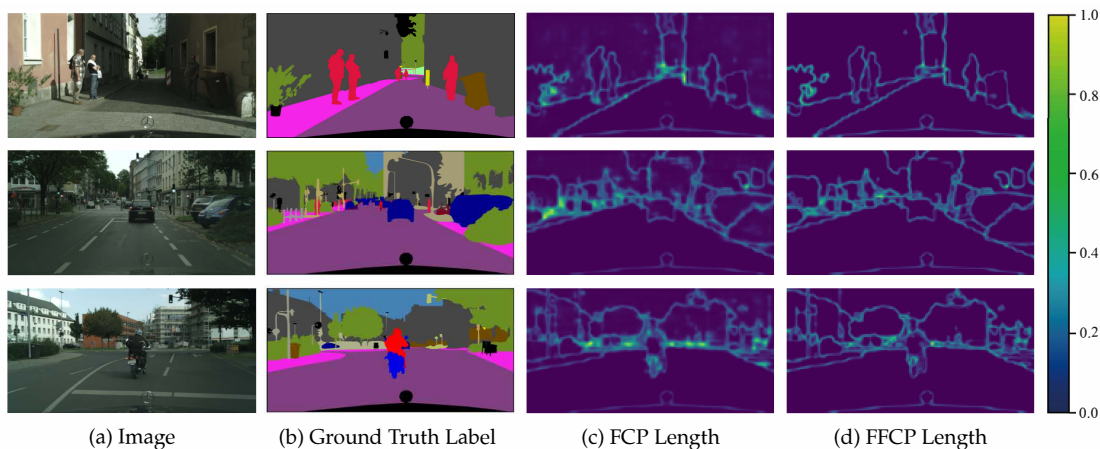


Figure 2: The results of FFCP and FCP in image segmentation tasks show that brighter regions indicate areas of uncertainty. Both FFCP and FCP highlight uncertain regions around the edges, which is informative. FFCP, however, returns bands with sharper boundaries.

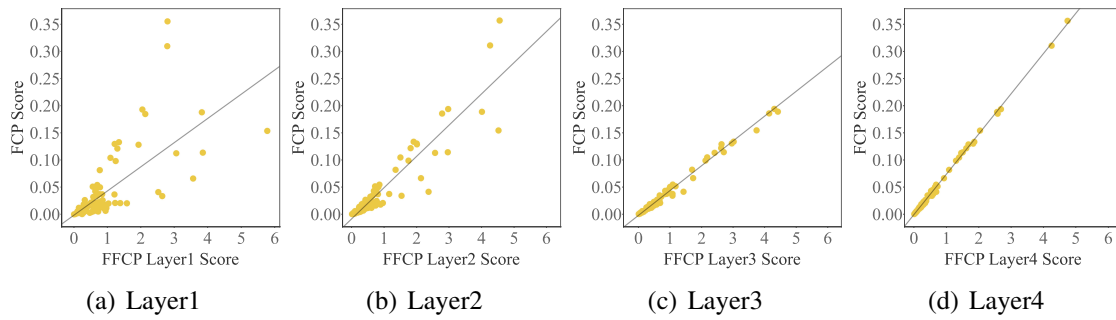


Figure 3: Scatter plot of FCP Score and FFCP Score at different Layers. The relationship between FCP Score and FFCP Score is positively correlated, which indicates that FFCP Score effectively replaces FCP Score.

References

- Michael I Jordan and Tom M Mitchell. Machine learning: Trends, perspectives, and prospects. *Science*, 349(6245):255–260, 2015.
- David Silver, Julian Schrittwieser, Karen Simonyan, Ioannis Antonoglou, Aja Huang, Arthur Guez, Thomas Hubert, Lucas Baker, Matthew Lai, Adrian Bolton, et al. Mastering the game of go without human knowledge. *nature*, 550(7676):354–359, 2017.
- Hongxin Wei, Renchunzi Xie, Hao Cheng, Lei Feng, Bo An, and Yixuan Li. Mitigating neural network overconfidence with logit normalization. In *International conference on machine learning*, pages 23631–23644. PMLR, 2022.
- Ziwei Ji, Nayeon Lee, Rita Frieske, Tiezheng Yu, Dan Su, Yan Xu, Etsuko Ishii, Ye Jin Bang, Andrea Madotto, and Pascale Fung. Survey of hallucination in natural language generation. *ACM Computing Surveys*, 55(12):1–38, 2023.
- Annetine C Gelijns, Joshua Graff Zivin, and Richard R Nelson. Uncertainty and technological change in medicine. *Journal of Health Politics, Policy and Law*, 26(5):913–924, 2001.
- Harsha Thirumurthy, David A Asch, and Kevin G Volpp. The uncertain effect of financial incentives to improve health behaviors. *Jama*, 321(15):1451–1452, 2019.
- Jonathan Morduch and Rachel Schneider. *The financial diaries: How American families cope in a world of uncertainty*. Princeton University Press, 2017.
- Moloud Abdar, Farhad Pourpanah, Sadiq Hussain, Dana Rezazadegan, Li Liu, Mohammad Ghavamzadeh, Paul Fieguth, Xiaochun Cao, Abbas Khosravi, U Rajendra Acharya, et al. A review of uncertainty quantification in deep learning: Techniques, applications and challenges. *Information fusion*, 76:243–297, 2021.
- Chuan Guo, Geoff Pleiss, Yu Sun, and Kilian Q. Weinberger. On calibration of modern neural networks. *ArXiv*, abs/1706.04599, 2017.
- Yanzhi Chen, Dinghuai Zhang, Michael U. Gutmann, Aaron Courville, and Zhanxing Zhu. Neural approximate sufficient statistics for implicit models. In *International Conference on Learning Representations*, 2021. URL <https://openreview.net/forum?id=SRDuJssQud>.
- Jakob Gawlikowski, Cedrique Rovile Njieutcheu Tassi, Mohsin Ali, Jongseok Lee, Matthias Humt, Jianxiang Feng, Anna M. Kruspe, Rudolph Triebel, Peter Jung, Ribana Roscher, Muhammad Shahzad, Wen Yang, Richard Bamler, and Xiao Xiang Zhu. A survey of uncertainty in deep neural networks. *CoRR*, abs/2107.03342, 2021. URL <https://arxiv.org/abs/2107.03342>.

- Vladimir Vovk, Alexander Gammerman, and Glenn Shafer. *Algorithmic learning in a random world*, volume 29. Springer, 2005.
- Glenn Shafer and Vladimir Vovk. A tutorial on conformal prediction. *Journal of Machine Learning Research*, 9(3), 2008a.
- Evgeny Burnaev and Vladimir Vovk. Efficiency of conformalized ridge regression. In *Conference on Learning Theory*, pages 605–622. PMLR, 2014.
- Yelong Shen, Xiaodong He, Jianfeng Gao, Li Deng, and Grégoire Mesnil. Learning semantic representations using convolutional neural networks for web search. In *Proceedings of the 23rd international conference on world wide web*, pages 373–374, 2014.
- Jiaye Teng, Chuan Wen, Dinghuai Zhang, Yoshua Bengio, Yang Gao, and Yang Yuan. Predictive inference with feature conformal prediction. *arXiv preprint arXiv:2210.00173*, 2022.
- Kaidi Xu, Zhouxing Shi, Huan Zhang, Yihan Wang, Kai-Wei Chang, Minlie Huang, Bhavya Kailkhura, Xue Lin, and Cho-Jui Hsieh. Automatic perturbation analysis for scalable certified robustness and beyond. *Advances in Neural Information Processing Systems*, 33:1129–1141, 2020.
- Yaniv Romano, Evan Patterson, and Emmanuel Candes. Conformalized quantile regression. *Advances in neural information processing systems*, 32, 2019a.
- Leying Guan. Localized conformal prediction: A generalized inference framework for conformal prediction. *Biometrika*, 110(1):33–50, 2023.
- Anastasios Angelopoulos, Stephen Bates, Jitendra Malik, and Michael I Jordan. Uncertainty sets for image classifiers using conformal prediction. *arXiv preprint arXiv:2009.14193*, 2020.
- Glenn Shafer and Vladimir Vovk. A tutorial on conformal prediction. *J. Mach. Learn. Res.*, 9:371–421, 2008b. URL <https://dl.acm.org/citation.cfm?id=1390693>.
- Rina Foygel Barber, Emmanuel J. Candès, Aaditya Ramdas, and Ryan J. Tibshirani. The limits of distribution-free conditional predictive inference. *Information and Inference: A Journal of the IMA*, 2020.
- Fanghua Ye, Mingming Yang, Jianhui Pang, Longyue Wang, Derek F Wong, Emine Yilmaz, Shuming Shi, and Zhaopeng Tu. Benchmarking llms via uncertainty quantification. *arXiv preprint arXiv:2401.12794*, 2024.
- Bhawesh Kumar, Charlie Lu, Gauri Gupta, Anil Palepu, David Bellamy, Ramesh Raskar, and Andrew Beam. Conformal prediction with large language models for multi-choice question answering. *arXiv preprint arXiv:2305.18404*, 2023.

- Victor Quach, Adam Fisch, Tal Schuster, Adam Yala, Jae Ho Sohn, Tommi S Jaakkola, and Regina Barzilay. Conformal language modeling. *arXiv preprint arXiv:2306.10193*, 2023.
- Ryan J. Tibshirani, Rina Foygel Barber, Emmanuel J. Candès, and Aaditya Ramdas. Conformal prediction under covariate shift. In Hanna M. Wallach, Hugo Larochelle, Alina Beygelzimer, Florence d’Alché-Buc, Emily B. Fox, and Roman Garnett, editors, *Advances in Neural Information Processing Systems 32: Annual Conference on Neural Information Processing Systems 2019, NeurIPS 2019, December 8-14, 2019, Vancouver, BC, Canada*, pages 2526–2536, 2019a. URL <https://proceedings.neurips.cc/paper/2019/hash/8fb21ee7a2207526da55a679f0332de2-Abstract.html>.
- Xiaoyu Hu and Jing Lei. A distribution-free test of covariate shift using conformal prediction. *arXiv: Methodology*, 2020.
- Aleksandr Podkopaev and Aaditya Ramdas. Distribution-free uncertainty quantification for classification under label shift. In *UAI*, 2021.
- Rina Foygel Barber, Emmanuel J Candès, Aaditya Ramdas, and Ryan J Tibshirani. Conformal prediction beyond exchangeability. *arXiv preprint arXiv:2202.13415*, 2022.
- Yaniv Romano, Matteo Sesia, and Emmanuel J. Candès. Classification with valid and adaptive coverage. *arXiv: Methodology*, 2020.
- Chen Xu and Yao Xie. Conformal prediction interval for dynamic time-series. In *ICML*, 2021.
- Isaac Gibbs and Emmanuel J. Candès. Adaptive conformal inference under distribution shift. In *NeurIPS*, 2021.
- Jiaye Teng, Zeren Tan, and Yang Yuan. T-SCI: A two-stage conformal inference algorithm with guaranteed coverage for cox-mlp. In Marina Meila and Tong Zhang, editors, *Proceedings of the 38th International Conference on Machine Learning, ICML 2021, 18-24 July 2021, Virtual Event*, volume 139 of *Proceedings of Machine Learning Research*, pages 10203–10213. PMLR, 2021. URL <http://proceedings.mlr.press/v139/teng21a.html>.
- Emmanuel Candès, Lihua Lei, and Zhimei Ren. Conformalized survival analysis. *Journal of the Royal Statistical Society Series B: Statistical Methodology*, 85(1):24–45, 2023.
- Emmanuel J Candès, Lihua Lei, and Zhimei Ren. Conformalized survival analysis. *arXiv preprint arXiv:2103.09763*, 2021.

- Jing Lei, Alessandro Rinaldo, and Larry A. Wasserman. A conformal prediction approach to explore functional data. *Annals of Mathematics and Artificial Intelligence*, 74:29–43, 2013.
- Zitong Yang, Emmanuel Candès, and Lihua Lei. Bellman conformal inference: Calibrating prediction intervals for time series. *arXiv preprint arXiv:2402.05203*, 2024.
- Lihua Lei and Emmanuel J. Candès. Conformal inference of counterfactuals and individual treatment effects. *Journal of the Royal Statistical Society: Series B (Statistical Methodology)*, 83, 2021.
- Harris Papadopoulos, Vladimir Vovk, and Alexander Gammerman. Regression conformal prediction with nearest neighbours. *J. Artif. Intell. Res.*, 40:815–840, 2011a. URL <http://jair.org/papers/paper3198.html>.
- Yaniv Romano, Evan Patterson, and Emmanuel J. Candès. Conformalized quantile regression. In Hanna M. Wallach, Hugo Larochelle, Alina Beygelzimer, Florence d’Alché-Buc, Emily B. Fox, and Roman Garnett, editors, *Advances in Neural Information Processing Systems 32: Annual Conference on Neural Information Processing Systems 2019, NeurIPS 2019, December 8-14, 2019, Vancouver, BC, Canada*, pages 3538–3548, 2019b. URL <https://proceedings.neurips.cc/paper/2019/hash/5103c3584b063c431bd1268e9b5e76fb-Abstract.html>.
- Matteo Sesia and Emmanuel J Candès. A comparison of some conformal quantile regression methods. *Stat*, 9(1):e261, 2020.
- Rafael Izbicki, Gilson T. Shimizu, and Rafael Bassi Stern. Distribution-free conditional predictive bands using density estimators. *ArXiv*, abs/1910.05575, 2020a.
- Matteo Sesia and Yaniv Romano. Conformal prediction using conditional histograms. In Marc’Aurelio Ranzato, Alina Beygelzimer, Yann N. Dauphin, Percy Liang, and Jennifer Wortman Vaughan, editors, *Advances in Neural Information Processing Systems 34: Annual Conference on Neural Information Processing Systems 2021, NeurIPS 2021, December 6-14, 2021, virtual*, pages 6304–6315, 2021. URL <https://proceedings.neurips.cc/paper/2021/hash/31b3b31a1c2f8a370206f111127c0dbd-Abstract.html>.
- Rafael Izbicki, Gilson Shimizu, and Rafael B Stern. Cd-split and hpd-split: efficient conformal regions in high dimensions. *arXiv preprint arXiv:2007.12778*, 2020b.
- Yachong Yang and Arun Kumar Kuchibhotla. Finite-sample efficient conformal prediction. *arXiv preprint arXiv:2104.13871*, 2021.
- Xing Han, Ziyang Tang, Joydeep Ghosh, and Qiang Liu. Split localized conformal prediction. *arXiv preprint arXiv:2206.13092*, 2022.

- Harris Papadopoulos, Alex Gammerman, and Volodya Vovk. Normalized nonconformity measures for regression conformal prediction. In *Proceedings of the IASTED International Conference on Artificial Intelligence and Applications (AIA 2008)*, pages 64–69, 2008.
- Harris Papadopoulos, Vladimir Vovk, and Alex Gammerman. Regression conformal prediction with nearest neighbours. *Journal of Artificial Intelligence Research*, 40: 815–840, 2011b.
- Harris Papadopoulos and Haris Haralambous. Reliable prediction intervals with regression neural networks. *Neural Networks*, 24(8):842–851, 2011.
- Nabeel Seedat, Alan Jeffares, Fergus Imrie, and Mihaela van der Schaar. Improving adaptive conformal prediction using self-supervised learning. In *International Conference on Artificial Intelligence and Statistics*, pages 10160–10177. PMLR, 2023.
- Nabeel Seedat, Jonathan Crabbé, Zhaozhi Qian, and Mihaela van der Schaar. Triage: Characterizing and auditing training data for improved regression. *Advances in Neural Information Processing Systems*, 36, 2024.
- Volodymyr Kuleshov, Nathan Fenner, and Stefano Ermon. Accurate uncertainties for deep learning using calibrated regression. In Jennifer G. Dy and Andreas Krause, editors, *Proceedings of the 35th International Conference on Machine Learning, ICML 2018, Stockholmsmässan, Stockholm, Sweden, July 10-15, 2018*, volume 80 of *Proceedings of Machine Learning Research*, pages 2801–2809. PMLR, 2018. URL <http://proceedings.mlr.press/v80/kuleshov18a.html>.
- Jeremy Nixon, Michael W. Dusenberry, Linchuan Zhang, Ghassen Jerfel, and Dustin Tran. Measuring calibration in deep learning. In *IEEE Conference on Computer Vision and Pattern Recognition Workshops, CVPR Workshops 2019, Long Beach, CA, USA, June 16-20, 2019*, pages 38–41. Computer Vision Foundation / IEEE, 2019. URL http://openaccess.thecvf.com/content_CVPRW_2019/html/Uncertainty_and_Robustness_in_Deep_Visual_Learning/Nixon_Measuring_Calibration_in_Deep_Learning_CVPRW_2019_paper.html.
- Yupeng Chang, Xu Wang, Jindong Wang, Yuan Wu, Linyi Yang, Kaijie Zhu, Hao Chen, Xiaoyuan Yi, Cunxiang Wang, Yidong Wang, et al. A survey on evaluation of large language models. *ACM Transactions on Intelligent Systems and Technology*, 15(3):1–45, 2024.
- Charles Blundell, Julien Cornebise, Koray Kavukcuoglu, and Daan Wierstra. Weight uncertainty in neural network. In Francis R. Bach and David M. Blei, editors, *Proceedings of the 32nd International Conference on Machine Learning, ICML 2015, Lille, France, 6-11 July 2015*, volume 37 of *JMLR Workshop and Conference Proceedings*, pages

- 1613–1622. JMLR.org, 2015. URL <http://proceedings.mlr.press/v37/blundell15.html>.
- José Miguel Hernández-Lobato and Ryan P. Adams. Probabilistic backpropagation for scalable learning of bayesian neural networks. In Francis R. Bach and David M. Blei, editors, *Proceedings of the 32nd International Conference on Machine Learning, ICML 2015, Lille, France, 6-11 July 2015*, volume 37 of *JMLR Workshop and Conference Proceedings*, pages 1861–1869. JMLR.org, 2015. URL <http://proceedings.mlr.press/v37/hernandez-lobatoc15.html>.
- Yingzhen Li and Yarin Gal. Dropout inference in bayesian neural networks with alpha-divergences. In Doina Precup and Yee Whye Teh, editors, *Proceedings of the 34th International Conference on Machine Learning, ICML 2017, Sydney, NSW, Australia, 6-11 August 2017*, volume 70 of *Proceedings of Machine Learning Research*, pages 2052–2061. PMLR, 2017. URL <http://proceedings.mlr.press/v70/li17a.html>.
- Pavel Izmailov, Sharad Vikram, Matthew D Hoffman, and Andrew Gordon Gordon Wilson. What are bayesian neural network posteriors really like? In *International conference on machine learning*, pages 4629–4640. PMLR, 2021.
- Laurent Valentin Jospin, Hamid Laga, Farid Boussaid, Wray Buntine, and Mohammed Bennamoun. Hands-on bayesian neural networks—a tutorial for deep learning users. *IEEE Computational Intelligence Magazine*, 17(2):29–48, 2022.
- Arthur U. Asuncion. Uci machine learning repository, university of california, irvine, school of information and computer sciences. 2007.
- Joel W. Cohen, Steven B. Cohen, and Jessica S. Banthin. The medical expenditure panel survey: A national information resource to support healthcare cost research and inform policy and practice. *Medical Care*, 47:S44–S50, 2009.
- CM Achilles, Helen Pate Bain, Fred Bellott, Jayne Boyd-Zaharias, Jeremy Finn, John Folger, John Johnston, and Elizabeth Word. Tennessee’s student teacher achievement ratio (star) project. *Harvard Dataverse*, 1:2008, 2008.
- Krisztian Buza. Feedback prediction for blogs. In *Data analysis, machine learning and knowledge discovery*, pages 145–152. Springer, 2014.
- Marius Cordts, Mohamed Omran, Sebastian Ramos, Timo Rehfeld, Markus Enzweiler, Rodrigo Benenson, Uwe Franke, Stefan Roth, and Bernt Schiele. The cityscapes dataset for semantic urban scene understanding. In *Proc. of the IEEE Conference on Computer Vision and Pattern Recognition (CVPR)*, 2016.
- Ryan J Tibshirani, Rina Foygel Barber, Emmanuel Candes, and Aaditya Ramdas. Conformal prediction under covariate shift. *Advances in neural information processing systems*, 32, 2019b.

Appendix

The complete proofs are presented in Section A, and the experiment details are outlined in Section B.

A Theoretical Proofs

We prove the theoretical guarantee for FFPC concerning coverage (effectiveness) in Section A.1 and band length (efficiency) in Section A.2.

A.1 Proofs of Theorem 4

The proof is based on the exchangeability of data (Assumption 1) on the calibration fold and test fold, hence the key step we need to derive is the exchangeability of the non-conformity scores $s_{\text{ff}}(X, Y, g \circ h) = |Y - f(X)| / \|\nabla g(\hat{v})\|$. We define the relevant symbols: \mathcal{D}_{tra} represents the train fold, \mathcal{D}_{tes} represents the test fold, \mathcal{D}_{cal} represents the calibration fold, and $\mathcal{D}' = \{(X_i, Y_i)\}_{i \in [m]}$ is the intersection of the two folds. m is the number of data points in \mathcal{D}' .

Similar to Teng et al. (2022), we first prove that for any function $\tilde{h} : \mathcal{X} \times \mathcal{Y} \rightarrow \mathbb{R}$, which is independent of \mathcal{D}' , $\tilde{h}(X_i, Y_i)$ satisfies exchangeability. For the CDF F_R of \tilde{h} and its perturbation CDF F_R^π , π is a random perturbation. We can conclude,

$$\begin{aligned}
 & F_R(u_1, \dots, u_n \mid \mathcal{D}_{\text{tra}}) \\
 &= \mathbb{P}(\tilde{h}(X_1, Y_1) \leq u_1, \dots, \tilde{h}(X_n, Y_n) \leq u_n \mid \mathcal{D}_{\text{tra}}) \\
 &= \mathbb{P}((X_1, Y_1) \in \mathcal{C}_{\tilde{h}-1}(u_1-), \dots, (X_n, Y_n) \in \mathcal{C}_{\tilde{h}-1}(u_n-) \mid \mathcal{D}_{\text{tra}}) \\
 &= \mathbb{P}((X_{\pi(1)}, Y_{\pi(1)}) \in \mathcal{C}_{\tilde{h}-1}(u_1-), \dots, (X_{\pi(n)}, Y_{\pi(n)}) \in \mathcal{C}_{\tilde{h}-1}(u_n-) \mid \mathcal{D}_{\text{tra}}) \quad (13) \\
 &= \mathbb{P}(\tilde{h}(X_{\pi(1)}, Y_{\pi(1)}) \leq u_1, \dots, \tilde{h}(X_{\pi(n)}, Y_{\pi(n)}) \leq u_n \mid \mathcal{D}_{\text{tra}}) \\
 &= F_R^\pi(u_1, \dots, u_n \mid \mathcal{D}_{\text{tra}}),
 \end{aligned}$$

where $\mathcal{C}_{\tilde{h}-1}(u-) = \{(X, Y) : \tilde{h}(X, Y) \leq u\}$.

Next, we need to show the non-conformity score function

$$s_{\text{ff}}(X, Y, g \circ h) = |Y - f(X)| / \|\nabla g(\hat{v})\|, \quad (14)$$

which is independent of the dataset \mathcal{D}' .

We can see that the non-conformity score $s_{\text{ff}}(X, Y, g \circ h)$ on \mathcal{D}' uses information from g and h , both of which depend only on the training set \mathcal{D}_{tra} . Moreover, calculating this

non-conformity score in the Algorithm 2 uses only single-point information, not the entire dataset \mathcal{D}' .

By integrating the aforementioned, we deduce that the non-conformity scores $s_{\text{ff}}(X, Y, g \circ h)$ on \mathcal{D}' exhibit exchangeability. This exchangeability, as per Lemma 1 in Tibshirani et al. (2019b), lends theoretical support to the efficacy of FFCP.

A.2 Proofs of Theorem 6

Our main conclusions are inspired by Theorem 4 in Teng et al. (2022). The details are as follows

Definitions. Let \mathcal{P} denote the overall population distribution. The calibration set \mathcal{D}_{cal} consists of n samples drawn from \mathcal{P} . We denote the specific distribution of these samples as \mathcal{P}^n . The model under consideration, $f = g \circ h$, includes h as the feature extractor and g as the prediction head, with g assumed to be a continuous function. $V_{\mathcal{D}}^o$ represent the individual length in output space, given data set \mathcal{D} . The term $Q_{1-\alpha}(R)$ represents the $(1 - \alpha)$ -quantile of the set R , which adjusted to include the value 0. Furthermore, $\mathbb{M}[\cdot]$ signifies the mean value of a set, and subtracting a real number from a set indicates that the subtraction is applied uniformly to all elements within the set.

Vanilla CP. Let $V_{\mathcal{D}_{\text{cal}}}^o = \{v_i^o\}_{i \in \mathcal{I}_{\text{cal}}}$ denote the individual length in the output space for vanilla CP, given the calibration set \mathcal{D}_{cal} . Since vanilla CP returns band length with $1 - \alpha$ quantile of non-conformity score, the resulting average band length is derived by $2Q_{1-\alpha}(V_{\mathcal{D}_{\text{cal}}}^o)$.

Fast Feature CP. According to the definition of FFCP, $V_{\mathcal{D}}^f = V_{\mathcal{D}}^o / \|\nabla g(\hat{v})\|$,

The resulting band length in FFCP is denoted by $2\mathbb{E}_{(X', Y') \sim \mathcal{P}}(\|\nabla g(\hat{v}')\| \cdot Q_{1-\alpha}(V_{\mathcal{D}_{\text{cal}}}^o / \|\nabla g(\hat{v}_{\text{cal}})\|)$.

Theorem 6. (*FFCP is provably more efficient*). Assume that the non-conformity score is in norm-type. We assume a Holder assumption that there exist $\alpha > 0, L > 0$ such that $|\mathcal{H}(x; X) - \mathcal{H}(y; X)| \leq L|x - y|^\alpha$ for all X , where \mathcal{H} is any function. Then the feature space satisfies the following square conditions:

1. **Expansion.** The feature space expands the differences between individual length and their quantiles, namely, $L\mathbb{E}_{\mathcal{D} \sim \mathcal{P}^n} \mathbb{M}[Q_{1-\alpha}(V_{\mathcal{D}}^o / \|\nabla g(\hat{v})\|) - V_{\mathcal{D}}^o / \|\nabla g(\hat{v})\|]^\alpha < \mathbb{E}_{\mathcal{D} \sim \mathcal{P}^n} \mathbb{M}[Q_{1-\alpha}(V_{\mathcal{D}}^o) - V_{\mathcal{D}}^o] - 2 \max\{L, 1\}(c/\sqrt{n})^{\min\{\alpha, 1\}}$.
2. **Quantile Stability.** Given a calibration set \mathcal{D}_{cal} , the quantile of the band length is stable in both feature space and output space, namely, $\mathbb{E}_{\mathcal{D} \sim \mathcal{P}^n} |Q_{1-\alpha}(V_{\mathcal{D}}^o / \|\nabla g(\hat{v})\|) - Q_{1-\alpha}(V_{\mathcal{D}_{\text{cal}}}^o / \|\nabla g(\hat{v}_{\text{cal}})\|)| \leq \frac{c}{\sqrt{n}}$ and $\mathbb{E}_{\mathcal{D} \sim \mathcal{P}^n} |Q_{1-\alpha}(V_{\mathcal{D}}^o) - Q_{1-\alpha}(V_{\mathcal{D}_{\text{cal}}}^o)| \leq \frac{c}{\sqrt{n}}$.

Then FFCP provably outperforms vanilla CP in terms of average band length, namely,

$$\mathbb{E}_{(X', Y') \sim \mathcal{P}}(\|\nabla g(\hat{v}')\| \cdot Q_{1-\alpha}(V_{\mathcal{D}_{cal}}^o / \|\nabla g(\hat{v}_{cal})\|) < Q_{1-\alpha}(V_{\mathcal{D}_{cal}}^o),$$

where the expectation is taken over the calibration fold and the testing point (X', Y') .

Proof of Theorem 6. We first proof with *Expansion Assumption*,

$$\begin{aligned} L\mathbb{E}_{\mathcal{D} \sim \mathcal{P}^n} \mathbb{M}|Q_{1-\alpha}(V_{\mathcal{D}}^o / \|\nabla g(\hat{v})\|) - V_{\mathcal{D}}^o / \|\nabla g(\hat{v})\||^\alpha &< \mathbb{E}_{\mathcal{D} \sim \mathcal{P}^n} \mathbb{M}[Q_{1-\alpha}(V_{\mathcal{D}}^o) - V_{\mathcal{D}}^o] \\ &- 2 \max\{L, 1\} (c/\sqrt{n})^{\min\{\alpha, 1\}}. \end{aligned} \quad (15)$$

And we can obtain

$$\begin{aligned} \mathbb{E}_{\mathcal{D}} \mathbb{M} V_{\mathcal{D}}^o &< \mathbb{E}_{\mathcal{D}} Q_{1-\alpha}(V_{\mathcal{D}}^o) \\ &- 2 \max\{L, 1\} (c/\sqrt{n})^{\min\{\alpha, 1\}} - L\mathbb{E}_{\mathcal{D} \sim \mathcal{P}^n} \mathbb{M}|Q_{1-\alpha}(V_{\mathcal{D}}^o / \|\nabla g(\hat{v})\|) - V_{\mathcal{D}}^o / \|\nabla g(\hat{v})\||^\alpha. \end{aligned} \quad (16)$$

According to Holder condition for quantile function, we obtain that $\mathbb{M}(\|\nabla g(\hat{v})\| \cdot Q_{1-\alpha}(V_{\mathcal{D}}^o / \|\nabla g(\hat{v})\|)) \leq \mathbb{M} V_{\mathcal{D}}^o + L\mathbb{M}|Q_{1-\alpha}(V_{\mathcal{D}}^o / \|\nabla g(\hat{v})\|) - V_{\mathcal{D}}^o / \|\nabla g(\hat{v})\||^\alpha$, therefore

$$\mathbb{E}_{\mathcal{D}} \mathbb{M}(\|\nabla g(\hat{v})\| \cdot Q_{1-\alpha}(V_{\mathcal{D}}^o / \|\nabla g(\hat{v})\|)) < \mathbb{E}_{\mathcal{D}} Q_{1-\alpha}(V_{\mathcal{D}}^o) - 2 \max\{1, L\} [c/\sqrt{n}]^{\min\{1, \alpha\}}. \quad (17)$$

As the *Quantile Stability* assumption, we have that $\mathbb{E}_{\mathcal{D} \sim \mathcal{P}^n} |Q_{1-\alpha}(V_{\mathcal{D}}^o / \|\nabla g(\hat{v})\|) - Q_{1-\alpha}(V_{\mathcal{D}_{cal}}^o / \|\nabla g(\hat{v}_{cal})\|)| \leq \frac{c}{\sqrt{n}}$ and $\mathbb{E}_{\mathcal{D} \sim \mathcal{P}^n} |Q_{1-\alpha}(V_{\mathcal{D}}^o) - Q_{1-\alpha}(V_{\mathcal{D}_{cal}}^o)| \leq \frac{c}{\sqrt{n}}$. Therefore,

$$\begin{aligned} &2\mathbb{E}(\|\nabla g(\hat{v})\| \cdot Q_{1-\alpha}(V_{\mathcal{D}_{cal}}^o / \|\nabla g(\hat{v}_{cal})\|)) \\ &< 2Q_{1-\alpha}(V_{\mathcal{D}}^o) - 2 \max\{1, L\} [c/\sqrt{n}]^{\min\{1, \alpha\}}. \\ &< 2Q_{1-\alpha}(V_{\mathcal{D}}^o). \end{aligned} \quad (18)$$

□

B Experimental Details

Section B.1 introduces the omitted experimental details. Section B.2 certifies the square conditions. Section B.3 discusses discusses the robustness of FFCP coverage with respect to the splitting point and across each network layer. Section B.4 demonstrates that FFCP performs similarly to vanilla CP in untrained neural networks, confirming that FFCP's efficiency is due to the semantic information trained in the feature space. Section B.5 proposes FFCQR after applying the gradient-level techniques of FFCP to CQR. Section B.6 proposes FFLCP after applying the gradient-level techniques of FFCP to LCP. Section B.7 proposes FFRAPS after applying the gradient-level techniques of FFCP to RAPS. Finally, Section B.8 provides additional experimental results.

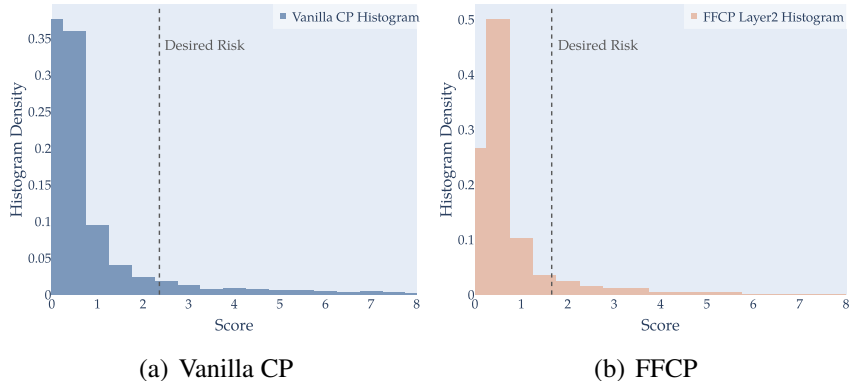


Figure 4: Empirical validation of Theorem 6. We plot the score distributions and their corresponding quantiles ($\alpha = 0.1$) of Vanilla CP (left) and FFCP (right). Compared to Vanilla CP, the non-conformity scores of FFCP are closer to their quantiles, leading to a shorter band. Compared to Vanilla, FFCP exhibits a more stable distribution with higher quantiles, leading to better performance for FFCP. FFCP selects layer 2 for display.

B.1 Experimental Details

Model Architecture. For the one-dimensional we employ a four-layer neural network, with each layer consisting of 64 dimensions. For the semantic segmentation experiment, we utilize a network architecture combining ResNet50 with two additional convolutional layers. We use ResNet50 as the base feature extractor h , and the two subsequent convolution layers form the prediction head g .

B.2 Verifying Square Conditions

We verify the square conditions in this section. The key component of the square conditions is *Expansion* condition, which states that performing the quantile step does not result in a significant loss of efficiency.

For computational simplicity, We take exponent $\alpha = 1$ and do not consider the Lipschitz factor L . We next provide experiment results in Figure 4 on comparing the distribution of the scores between Vanilla CP with FFCP.

From the figure, we observe that the overall distribution of FFCP non-conformity scores is closer to the quantile. This numerically validates that $\mathbf{M} [Q_{1-\alpha}(V_{\mathcal{D}}^o/|\nabla g(\hat{v})|) - V_{\mathcal{D}}^o/|\nabla g(\hat{v})|]$ is less than $\mathbf{M} [Q_{1-\alpha}(V_{\mathcal{D}}^o) - V_{\mathcal{D}}^o]$.

B.3 Robustness of FFCP

To verify that the coverage by FFCP maintains its robustness despite changes in the splitting point, we performed a network split. The experimental results, detailed in Table 7, demonstrate that FFCP is indeed robust.

Table 7: Ablation study of the number of layers in h and g in unidimensional tasks. For the sake of avoiding redundancy, we set $\alpha = 0.05$.

DATASET		FACEBOOK1		MEPS19		BLOG	
METHOD	NUMBER($\hat{g} \circ \hat{h}$)	COVERAGE	LENGTH	COVERAGE	LENGTH	COVERAGE	LENGTH
VANILLA CP	/	95.24 ± 0.16	4.60 ± 0.50	95.35 ± 0.23	7.34 ± 1.01	95.08 ± 0.11	7.88 ± 0.97
FFCP	$h : 0 \quad g : 4$	94.88 ± 0.19	5.35 ± 0.42	95.18 ± 0.40	5.36 ± 0.52	94.97 ± 0.31	8.28 ± 0.59
	$h : 1 \quad g : 3$	94.84 ± 0.14	4.21 ± 0.46	95.13 ± 0.38	5.15 ± 0.49	94.99 ± 0.18	6.37 ± 1.22
	$h : 2 \quad g : 2$	95.14 ± 0.13	2.48 ± 0.09	95.19 ± 0.36	5.57 ± 0.87	95.08 ± 0.12	5.36 ± 0.93
	$h : 3 \quad g : 1$	95.16 ± 0.18	2.59 ± 0.72	95.34 ± 0.22	6.95 ± 1.13	95.05 ± 0.11	6.46 ± 1.52
	$h : 4 \quad g : 0$	95.24 ± 0.16	4.60 ± 0.50	95.35 ± 0.23	7.34 ± 1.01	95.08 ± 0.11	7.88 ± 0.97

B.4 FFCP works due to semantic information in feature space

One of our primary advantages is that FFCP leverages the semantic information of gradient in feature space. This is due to the fact that gradient-level techniques in feature space improve efficiency via the robust feature embedding abilities of well-trained neural networks.

On the other hand, when the base model is untrained and initialized randomly, lacking meaningful semantic representation in gradient, the band length produced by FFCP is comparable to Vanilla CP. For results, see Table 6.

B.5 FFCQR

This section highlights the adaptability of FFCP’s gradient-level techniques, showing their suitability for a wide range of existing conformal prediction algorithms. We choose Conformalized Quantile Regression (CQR, Romano et al. (2019b)) to propose Fast Feature Conformalized Quantile Regression (FFCQR). The fundamental concept is similar to FFCP Algorithm 2, where calibration steps are performed within the gradient information. FFCQR algorithm is proposed in Algorithm 3.

We summarize run time in Table 8 and the experiments result in Table 9 (meps19), Table 10 (com), and Table 11 (bike). FFCQR reduces runtime compared to FCQR, while achieving better efficiency compared to CQR.

Furthermore, we have observed that as the values of $[\alpha, 1 - \alpha]$ used by the neural networks in all CQR methods (CQR, FCQR and FFCQR) become increasingly closer in the training

Algorithm 3 Fast Feature Conformalized Quantile Regression (FFCQR)

Input: Confidence level α , dataset $\mathcal{D} = \{(X_i, Y_i)\}_{i \in \mathcal{I}}$, test point X' ;

- 1: Randomly split the dataset \mathcal{D} into a training fold $\mathcal{D}_{\text{tra}} \triangleq (X_i, Y_i)_{i \in \mathcal{I}_{\text{tra}}}$ together with a calibration fold $\mathcal{D}_{\text{cal}} \triangleq (X_i, Y_i)_{i \in \mathcal{I}_{\text{cal}}}$;
- 2: Train a base machine learning model $f^{\text{lo}} = g^{\text{lo}} \circ h(\cdot)$ and $f^{\text{hi}} = g^{\text{hi}} \circ h(\cdot)$ using \mathcal{D}_{tra} to estimate the quantile of response Y_i , which returns $[f^{\text{lo}}(X_i), f^{\text{hi}}(X_i)]$;
- 3: For each $i \in \mathcal{I}_{\text{cal}}$, calculate the non-conformity score $\tilde{R}_i^{\text{lo}} = (f^{\text{lo}}(X_i) - Y_i) / \|\nabla g^{\text{lo}}(\hat{v}_i)\|$ and $\tilde{R}_i^{\text{hi}} = (Y_i - f^{\text{hi}}(X_i)) / \|\nabla g^{\text{hi}}(\hat{v}_i)\|$, where $\nabla g(\cdot)$ denote the gradient of $g(\cdot)$ on the feature $\hat{v}_i \triangleq h(X_i)$, namely $\nabla g^{\text{lo}}(\hat{v}_i) = \frac{dg^{\text{lo}} \circ h(X_i)}{dh(X_i)}$ and $\nabla g^{\text{hi}}(\hat{v}_i) = \frac{dg^{\text{hi}} \circ h(X_i)}{dh(X_i)}$;
- 4: Calculate the $(1 - \alpha)$ -th quantile $Q_{1-\alpha}$ of the distribution $\frac{1}{|\mathcal{I}_{\text{cal}}|+1} \sum_{i \in \mathcal{I}_{\text{cal}}} \delta_{\tilde{R}_i} + \delta_{\infty}$, where $\tilde{R}_i = \max\{\tilde{R}_i^{\text{lo}}, \tilde{R}_i^{\text{hi}}\}$

Output: $\mathcal{C}_{1-\alpha}^{\text{ffcqr}}(X') = [f^{\text{lo}}(X') - \|\nabla g^{\text{lo}}(\hat{v}')\| \cdot Q_{1-\alpha}, f^{\text{hi}}(X') + \|\nabla g^{\text{hi}}(\hat{v}')\| \cdot Q_{1-\alpha}]$, where $\hat{v}' = h(X')$.

process (The level difference between [0.1, 0.9] is 0.8, while the level difference between [0.49, 0.51] is 0.02, with the difference gradually decreasing), the band length returned by FFCQR gradually narrows. This implies that our method holds an advantage on returned band length when the narrower neural network confidence level.

Table 8: Time Comparison among CQR, FCQR and FFCQR. For quantile regression tasks, FFCQR also demonstrates more efficient performance. The last column represents the speed improvement factor of FFCQR compared to FCQR. The time unit is in seconds.

DATASET	CQR	FCQR	FFCQR	FASTER
SYNTHETIC	0.0125±0.0062	0.3237±0.0152	0.0742±0.0091	4X
COM	0.0045±0.0015	0.2730±0.1088	0.0210±0.0011	13X
FB1	0.0446±0.0157	1.7276±0.1389	0.2532±0.0166	7X
FB2	0.0812±0.0187	3.9967±0.7330	0.0617±0.0123	65X
MEPS19	0.0187±0.0018	0.7671±0.0438	0.1189±0.0048	6X
MEPS20	0.0438±0.0079	1.1876±0.2206	0.1505±0.0138	8X
MEPS21	0.0187±0.0027	0.8004±0.0657	0.1120±0.0053	7X
STAR	0.0047±0.0009	0.2352±0.0419	0.0214±0.0005	11X
BIO	0.0774±0.0541	6.9365±4.5494	0.6473±0.4879	11X
BLOG	0.1121±0.0153	1.9591±0.1346	0.3941±0.0618	5X
BIKE	0.0138±0.0045	1.8528±2.3969	0.2382±0.3261	6X

B.6 Group coverage

Group coverage is represented by the conditional probability $\mathbb{P}(Y \in \mathcal{C}(X)|X)$. The test dataset was categorized into three groups by splitting response Y based on the lower and

Table 9: Coverage and Band Length at Different Confidence Levels Used By the Neural Networks in CQR methods with *Meps19* dataset. FFCQR yields shorter band lengths compared to CQR.

CONFIDENCE LEVELS USED BY NN		[0.1, 0.9]		[0.2, 0.8]		[0.3, 0.7]		[0.4, 0.6]		[0.49, 0.51]	
METRICS		COVERAGE	LENGTH	COVERAGE	LENGTH	COVERAGE	LENGTH	COVERAGE	LENGTH	COVERAGE	LENGTH
VANILLA CQR		90.28±0.47	2.43±0.11	90.19±0.46	2.58±0.45	90.63±0.32	2.93±0.51	90.48±0.42	3.47±0.16	90.44±0.36	3.48±0.08
FCQR		91.32±0.37	1.50±0.37	90.26±0.33	2.61±2.01	90.45±0.54	2.30±2.38	90.58±0.33	6.11±0.89	90.47±0.45	4.59±1.73
	LAYER0	90.29±0.60	2.61±0.13	90.22±0.26	2.58±0.54	90.31±0.43	3.03±0.90	89.95±0.29	5.30±0.57	89.84±0.12	5.96±1.26
	LAYER1	90.29±0.57	2.56±0.13	90.10±0.33	2.49±0.52	90.34±0.46	2.92±0.85	90.02±0.33	5.07±0.50	89.88±0.24	5.71±1.22
FFCQR		90.14±0.60	2.34±0.12	90.24±0.65	2.22±0.32	90.34±0.43	2.60±0.68	89.96±0.40	4.10±0.22	89.97±0.33	4.76±1.17
	LAYER3	90.21±0.45	2.18±0.12	90.14±0.42	2.10±0.19	90.35±0.36	2.34±0.19	90.28±0.33	2.76±0.15	89.86±0.49	3.16±0.62
	LAYER4	90.28±0.47	2.43±0.11	90.19±0.46	2.58±0.45	90.63±0.32	2.93±0.51	90.48±0.42	3.47±0.16	90.44±0.36	3.48±0.08

Table 10: Coverage and Band Length at Different Confidence Levels Used By the Neural Networks in CQR methods with *com* dataset. FFCQR yields shorter band lengths compared to CQR.

CONFIDENCE LEVELS USED BY NN		[0.1, 0.9]		[0.2, 0.8]		[0.3, 0.7]		[0.4, 0.6]		[0.49, 0.51]	
METRICS		COVERAGE	LENGTH	COVERAGE	LENGTH	COVERAGE	LENGTH	COVERAGE	LENGTH	COVERAGE	LENGTH
VANILLA CQR		89.87±1.68	1.57±0.12	90.13±0.89	1.71±0.18	89.87±1.06	1.74±0.16	89.27±0.94	2.07±0.55	89.57±0.49	1.99±0.12
FCQR		90.83±1.53	1.19±0.19	90.43±1.32	0.49±0.38	90.23±1.13	0.37±0.06	90.18±1.77	0.20±0.05	89.47±0.85	0.23±0.07
	LAYER0	88.92±2.78	1.62±0.12	89.62±1.75	1.67±0.07	91.53±0.97	1.62±0.12	89.77±1.64	1.80±0.27	89.82±1.07	1.76±0.11
	LAYER1	88.67±2.40	1.59±0.12	89.57±1.03	1.64±0.08	90.58±1.21	1.57±0.13	89.82±1.75	1.78±0.33	89.12±1.40	1.74±0.09
FFCQR		89.77±2.14	1.58±0.12	89.92±1.98	1.63±0.12	90.53±0.43	1.64±0.14	89.67±1.28	1.89±0.38	88.77±0.75	1.78±0.11
	LAYER3	90.08±2.28	1.58±0.12	89.92±1.22	1.67±0.15	90.33±0.86	1.73±0.13	89.62±0.83	2.03±0.54	89.27±0.66	1.93±0.11
	LAYER4	89.87±1.68	1.57±0.12	90.13±0.89	1.71±0.18	89.87±1.06	1.74±0.16	89.27±0.94	2.07±0.55	89.57±0.49	1.99±0.12

upper tertiles, and we have reported the minimum coverage for each group.

We present our results in two parts: (a) we present the group coverage provided by Vanilla CP, FCP, FFCP, detailed in Table 13 and (b) the group coverage provided by LCP and FFLCP, as shown in Table 4.

Analyzing the experimental results, we believe that the group coverage achieved through gradient-level techniques in FFCP reflects an improvement over Vanilla CP, albeit with moderate overall performance. We note that the group coverage of gradient-level conformal prediction is contingent upon its vanilla version. That is, when the vanilla version demonstrates satisfying group coverage, the gradient-level version tends to mirror this result. Thus, despite FFCP outperforming Vanilla CP, the overall performance is still considered average.

LCP, developed specifically to enhance group coverage, inherently achieves higher coverage. Experimental results further reveal that FFLCP surpasses LCP, demonstrating the superiority of our gradient-level techniques.

Table 11: Coverage and Band Length at Different Confidence Levels Used By the Neural Networks in CQR methods with *bike* dataset. FFCQR yields shorter band lengths compared to CQR.

CONFIDENCE LEVELS USED BY NN	[0.1, 0.9]		[0.2, 0.8]		[0.3, 0.7]		[0.4, 0.6]		[0.49, 0.51]	
	COVERAGE	LENGTH	COVERAGE	LENGTH	COVERAGE	LENGTH	COVERAGE	LENGTH	COVERAGE	LENGTH
VANILLA CQR	89.38±0.73	0.82±0.07	89.99±0.69	0.73±0.03	89.63±0.84	0.77±0.03	90.25±0.62	0.84±0.02	89.72±0.51	0.96±0.08
FCQR	90.25±0.67	0.58±0.15	90.14±0.63	0.65±0.13	89.77±0.76	0.71±0.18	89.93±0.35	0.82±0.07	89.98±0.97	0.74±0.08
LAYER0	89.91±0.38	0.91±0.07	89.84±0.44	0.97±0.02	89.42±0.83	1.20±0.04	89.75±0.54	1.64±0.13	89.61±0.59	1.79±0.08
LAYER1	89.57±0.33	0.90±0.07	89.83±0.25	0.90±0.05	89.44±0.42	1.04±0.07	89.72±0.43	1.25±0.05	89.62±0.73	1.31±0.06
FFCQR	89.73±0.29	0.87±0.07	89.70±0.27	0.79±0.03	89.63±0.69	0.83±0.03	89.14±0.42	0.92±0.04	89.44±0.41	0.98±0.04
LAYER3	89.49±0.34	0.84±0.06	89.62±0.48	0.69±0.02	89.58±0.74	0.69±0.02	89.86±0.37	0.70±0.01	89.57±0.88	0.78±0.07
LAYER4	89.38±0.73	0.82±0.07	89.99±0.69	0.73±0.03	89.63±0.84	0.77±0.03	90.25±0.62	0.84±0.02	89.72±0.51	0.96±0.08

Table 12: Coverage and Band Length at Different Confidence Levels Used By the Neural Networks in CQR methods with *bio* dataset. FFCQR yields shorter band lengths compared to CQR.

CONFIDENCE LEVELS USED BY NN	[0.1, 0.9]		[0.2, 0.8]		[0.3, 0.7]		[0.4, 0.6]		[0.49, 0.51]	
	COVERAGE	LENGTH	COVERAGE	LENGTH	COVERAGE	LENGTH	COVERAGE	LENGTH	COVERAGE	LENGTH
VANILLA CQR	89.89±0.41	1.42±0.02	89.84±0.27	1.45±0.02	89.87±0.27	1.61±0.02	90.07±0.31	1.86±0.03	90.16±0.40	2.00±0.03
FCQR	90.18±0.35	0.95±0.50	90.45±0.45	2.09±0.41	90.16±0.48	1.84±0.43	90.25±0.46	2.37±0.76	90.21±0.46	2.02±0.34
LAYER0	89.74±0.32	1.47±0.01	89.98±0.22	1.56±0.04	89.89±0.25	1.73±0.04	89.87±0.24	2.22±0.15	89.64±0.20	2.55±0.06
LAYER1	89.77±0.33	1.45±0.01	89.99±0.21	1.48±0.03	89.92±0.37	1.59±0.03	89.92±0.21	1.99±0.12	89.69±0.28	2.21±0.04
FFCQR	89.77±0.40	1.43±0.02	90.01±0.23	1.41±0.01	90.02±0.32	1.49±0.03	90.01±0.49	1.76±0.11	89.79±0.35	1.94±0.07
LAYER3	89.75±0.41	1.41±0.02	89.98±0.34	1.38±0.02	89.93±0.41	1.47±0.01	90.07±0.12	1.68±0.04	89.97±0.34	1.78±0.02
LAYER4	89.89±0.41	1.42±0.02	89.84±0.27	1.45±0.02	89.87±0.27	1.61±0.02	90.07±0.31	1.86±0.03	90.16±0.40	2.00±0.03

B.7 FFRAPS

In this section, we show how to deploy gradient-level techniques in FFCP in classification problems. The basic ideas follow Algorithm 5.

Comparing to the experimental part of RAPS, our core adjustments are as follows:

(a) During the calibration process, for the model’s output of sorted scores s , we divide each element by the magnitude of its corresponding gradient: $s + \delta \cdot \|\nabla g(v)\|$. Here, δ is an adjustable hyper-parameter that can be tuned to optimize the performance of the model based on the specific characteristics of the data and the problem at hand.

(b) In the stage of calculating the returned set, we multiply the generalized inverse quantile τ by the magnitude of the gradient of the corresponding test data: $s' + \delta \cdot \|\nabla g(v')\|$

We summarize the experiment results in Table 3, where we adhere to the statistical methodologies of RAPS as described in Angelopoulos et al. (2020).

B.8 Additional Experiment Results

This section provides more experiment results. Additional visual results for the segmentation problem are also presented in Figure 5.

Table 13: Comparison of Vanilla CP, FCP and FFCP in group coverage.

METHOD	VANILLA CP	FCP	FFCP				
	COVERAGE	COVERAGE	LAYER0	LAYER1	LAYER2	LAYER3	LAYER4
SYNTHETIC	87.08±1.03	87.92±1.08	86.96±0.81	86.63±0.79	85.64±1.13	88.46 ±1.44	87.08±1.03
COM	79.41±3.12	79.57±2.96	82.00 ±3.18	79.41±3.62	78.64±4.35	78.65±3.62	79.41±3.12
FB1	56.69±1.35	57.34±1.12	79.20 ±0.95	76.75±1.42	68.09±1.76	59.33±1.91	56.69±1.35
FB2	57.98±1.28	58.72±0.87	76.27 ±0.92	75.64±0.91	70.86±0.89	62.43±1.15	57.98±1.28
MEPS19	73.78±1.08	73.82 ±0.91	70.90±2.29	70.51±2.28	72.09±1.25	73.53±1.00	73.78±1.08
MEPS20	72.21±1.47	72.33 ±1.46	70.42±0.88	70.13±1.42	69.51±0.79	71.17±2.01	72.21±1.47
MEPS21	71.38±0.20	72.02 ±0.70	69.40±1.61	69.83±1.44	69.81±1.68	70.85±0.82	71.39±0.20
STAR	83.45 ±3.09	83.17±3.47	82.89±1.51	81.22±2.55	81.22±3.60	83.03±2.07	83.45 ±3.09
BIO	81.00±0.61	84.45±0.88	87.31±0.27	87.27±0.46	88.31 ±0.72	84.20±0.70	81.00±0.61
BLOG	58.32±0.90	60.43±1.46	65.21 ±0.58	59.03±1.03	54.55±0.77	55.76±1.26	58.32±0.90
BIKE	77.55±1.40	86.25±0.87	95.36 ±1.32	94.23±1.40	95.06±1.06	84.65±1.85	77.55±1.40

Algorithm 4 Fast Feature Localized Conformal Prediction (FFLCP)

Input: Confidence level α , dataset $\mathcal{D} = \{(X_i, Y_i)\}_{i \in \mathcal{I}}$, testing point X' , localizer $D(X, Y)$

- 1: Randomly split the dataset \mathcal{D} into a training fold $\mathcal{D}_{\text{tra}} \triangleq \{(X_i, Y_i)\}_{i \in \mathcal{I}_{\text{tra}}}$ and a calibration fold $\mathcal{D}_{\text{cal}} \triangleq \{(X_i, Y_i)\}_{i \in \mathcal{I}_{\text{cal}}}$;
- 2: Train a base neural network with training fold $f(\cdot) = g \circ h(\cdot)$ with training fold \mathcal{D}_{tra} ;
- 3: For each $i \in \mathcal{I}_{\text{cal}}$, calculate the non-conformity score $\tilde{R}_i = |Y_i - f(X_i)| / \|\nabla g(\hat{v}_i)\|$, where $\nabla g(\hat{v}_i)$ denotes the gradient of $g(\cdot)$ on the feature $\hat{v}_i \triangleq h(X_i)$, namely $\nabla g(\hat{v}_i) = \frac{dg \circ h(X_i)}{dh(X_i)}$;
- 4: Calculate the distance $D_i \triangleq D(X', X_i)$, $d_i^D := \frac{D_i}{\sum_{i \in \mathcal{I}_{\text{cal}}} D_i}$ and $(1 - \alpha)$ -th quantile $Q_{1-\alpha}$ of the distribution $\sum_{i \in \mathcal{I}_{\text{cal}}} d_i^D \delta_{\tilde{R}_i} + \delta_\infty$;

Output: $\mathcal{C}_{1-\alpha}^{\text{fflcp}}(X') = [f(X') - \|\nabla g(\hat{v}')\|Q_{1-\alpha}, f(X') + \|\nabla g(\hat{v}')\|Q_{1-\alpha}]$, where $\hat{v}' = h(X')$.

Algorithm 5 Fast Feature Regularized Adaptive Prediction Sets (FFRAPs)

Input: Confidence level α , dataset $\mathcal{D} = \{(X_i, Y_i)\}_{i \in \mathcal{I}}$, testing point X' , and ground-truth label $y \in \{0, 1, \dots, K\}^n$ for $X \in \mathcal{D}$ and X' ; regularization hyperparameters k_{reg} , δ and λ ;

- 1: Randomly split the dataset \mathcal{D} into a training fold $\mathcal{D}_{tra} \triangleq \{(X_i, Y_i)\}_{i \in \mathcal{I}_{tra}}$ and a calibration fold $\mathcal{D}_{cal} \triangleq \{(X_i, Y_i)\}_{i \in \mathcal{I}_{cal}}$;
- 2: Train a base neural network with training fold $f(\cdot) = g \circ h(\cdot)$ with training fold \mathcal{D}_{tra} ;
- 3: For each $i \in \mathcal{I}_{cal}$, $L_i \leftarrow j$ such that $I_{i,j} = y_i$, where I represents the associated permutation of index. Calculate generalized inverse quantile conformity score $E_i = \sum_{j=1}^{L_i} s_{i,j} + \|\nabla g(\hat{v}_i)\| \cdot \delta + \lambda(L_i - k_{reg})^+$, where $\nabla g(\hat{v}_i)$ denotes the gradient of $g(\cdot)$ on the feature $\hat{v}_i \triangleq h(X_i)$, namely $\nabla g(\hat{v}_i) = \frac{dg \circ h(X_i)}{dh(X_i)}$, where $s \triangleq \text{sort} f(X)$ represents the sorted scores. Calculate $\hat{\tau}_{ccal} \leftarrow \lceil (1 - \alpha)(1 + n) \rceil$ largest value in $\{E_i\}_{i=1}^n$;
- 4: Calculate $L \leftarrow |\{j \in \mathcal{Y} : \sum_{i=1}^j s'_i + \|\nabla g(\hat{v}')\| \cdot \delta + \lambda(j - k_{reg})^+ \leq \hat{\tau}_{ccal}^*\}| + 1$, where $\hat{v}' = h(X')$ and $s' = \text{sort} f(X')$;

Output: $\mathcal{C}_{1-\alpha}^{\text{FFRAPs}}(X') = \{I_1, \dots, I_L\}$

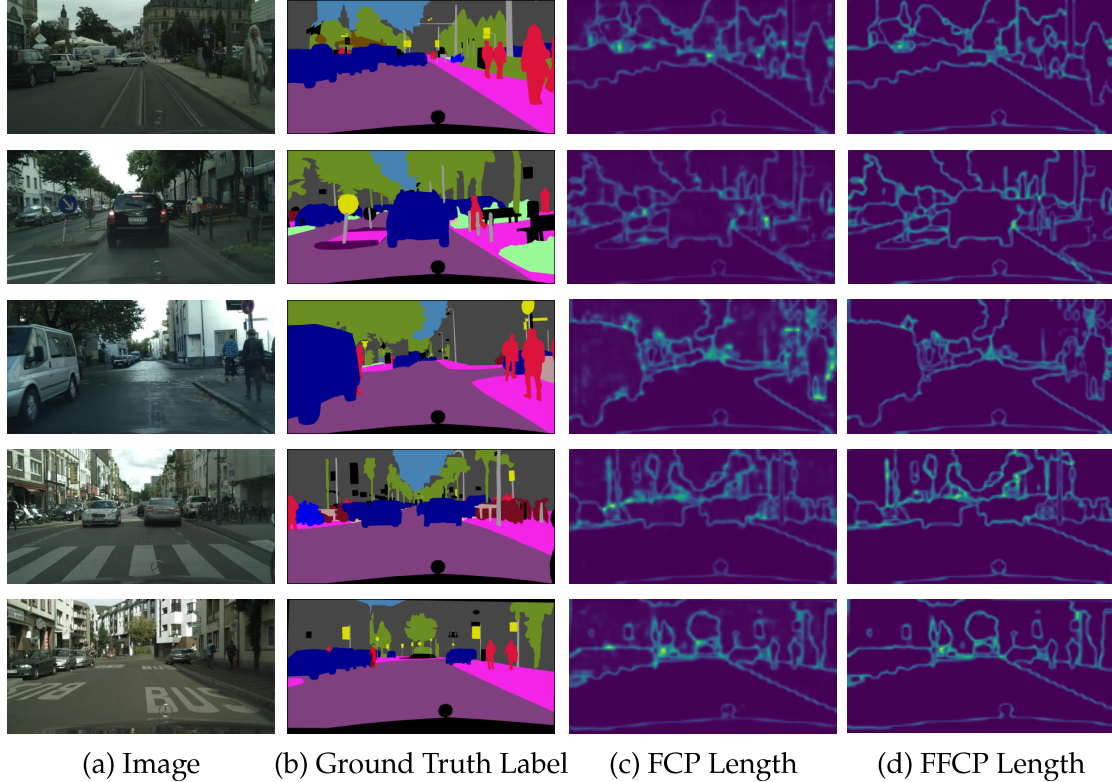


Figure 5: Additional visualization results in segmentation task.